Changes of regional meteorology induced by anthropogenic heat and their impacts on air quality in South China

Min Xie[1,2,3*], Kuanguang Zhu[1,5], Tijian Wang[1,3,4*], Wen Feng[2], Da Gao[1], Mengmeng Li[1], Shu Li[1], Bingliang Zhuang[1,3], Yong Han[1], Pulong Chen[1], Jingbiao Liao[1]

[1] School of Atmospheric Sciences, Nanjing University, Nanjing, China;

[2] Key Laboratory of South China Sea Meteorological Disaster Prevention and Mitigation of Hainan Province, Haikou, China

[3] Jiangsu Collaborative Innovation Center for Climate Change, Nanjing, China;

[4] CMA-NJU Joint Laboratory for Climate Prediction Studies, Institute for Climate and Global Change Research, School of Atmospheric Sciences, Nanjing University, Nanjing, China;

[5] Hubei Academy of Environmental Science, Wuhan, China

∗ Correspondence to: Min Xie (minxie@nju.edu.cn) and Tijian Wang (tjwang@nju.edu.cn)

Abstract: Anthropogenic heat (AH) emissions from human activities can change the urban circulation and thereby affect the air pollution in and around cities. Based on statistic data, the spatial distribution of AH flux in South China is estimated. With the aid of the WRF/Chem model in which the AH parameterization is developed to incorporate the gridded AH emissions with temporal variation, the simulations for January and July in 2014 are performed over South China. By analyzing the differences between the simulations with and without adding AH, the impact of AH on regional meteorology and air quality are quantified. The results show that the regional annual mean AH fluxes over South China are only 0.87W/m^2, but the values for the urban areas of the Pearl River Delta (PRD) region can be close to 60 W/m^2. These AH emissions can significantly change the urban heat island and urban-breeze circulations in the big cities. In the PRD city cluster, 2-m air temperature rises up by 1.1℃ in January and over 0.5℃ in July, the planetary boundary layer height (PBLH) increases by 120m in January and 90m in July, 10-m wind speed is intensified over 0.35 m/s in January and 0.3 m/s in July, and the accumulative precipitation is enhanced by 20-40% in July. These changes of meteorological conditions can significantly impact the spatial and vertical distributions of air pollutants. Due to the increases of PBLH, surface wind speed and upward vertical movement, the concentrations of primary air pollutants decrease near surface and increase at the upper levels. But the vertical changes of O_3 concentrations show the different patterns in different seasons. The surface O_3 concentrations in big cities increase with maximum values over 2.5ppb in January, while O_3 is reduced at the lower layers and increases at the upper layers above some megacities in July. This phenomenon should be attributed to the facts that the chemical effects can play a significant role in O_3 changes over South China in winter, while the vertical movement can be the dominant effect in some big cities in summer. Adding the gridded AH emissions can better describe the heterogeneous impacts of AH

on regional meteorology and air quality, suggesting that more studies on AH should be carried out in the climate and air quality assessments.

Key words: Anthropogenic heat; PRD; WRF/Chem; PM_{10}; O_3

Urbanization and its impacts on regional meteorology and air quality have been widely acknowledged, observed, and investigated (Rizwan et al., 2008; Mirzaei and Haghighat, 2010). Previous studies have illustrated that urbanization can affect atmospheric environment in many ways, which are mainly associated with the increase of air pollutant emissions from the intensification of energy consumptions (Akbari et al., 2001; Civerolo et al., 2007; Jiang et al, 2008; Stone, 2008; Chen et al., 2014b), the change of land covers from natural surfaces to artificial ones (Civerolo et al., 2007; Lo et al., 2007; Wang et al., 2007; 2009b; Jiang et al., 2008; Zhang et al., 2009a; Lu et al., 2010; Wu et al., 2011; Chen et al., 2014b; Liao et al., 2015; Zhu et al., 2015; Li et al., 2016), and the release of anthropogenic heat from human activities in cities (Ryu et al., 2013; Yu et al., 2014; Xie et al., 2016). Anthropogenic heat (AH) can increase turbulent fluxes in sensible and latent heat (Oke, 1988), implying that it can modulates local and regional meteorological processes (Ichinose et al., 1999; Block et al., 2004; Fan and Sailor, 2005; Ferguson and Woodbury, 2007; Chen et al., 2009; Zhu et al., 2010; Feng et al., 2012; 2014; Menberg et al., 2013; Ryu et al., 2013; Wu and Yang, 2013; Bohnenstengel et al., 2014; Chen et al., 2014a; Meng et al., 2011; Yu et al., 2014; Xie et al., 2016) and thereby exert an important influence on the formation and the distribution of ozone (Ryu et al., 2013; Yu et al., 2014; Xie et al., 2016) as well as aerosols (Yu et al., 2014; Xie et al., 2016).

Previous studies on AH basically focused on the amount of heat fluxes or their effects on meteorology. It was reported that the typical values of AH fluxes in urban areas range from 20 to 100 W/m^2 (Crutzen, 2004; Sailor and Lu, 2004; Fan and Sailor, 2005; Pigeon et al., 2007; Lee et al., 2009; Iamarino et al., 2012; Lu et al., 2016; Xie et al., 2016). Sometimes, the fluxes might exceed the value of 100 W/m^2 (Iamarino et al., 2012; Quah and Roth, 2012; Lu et al., 2016; Xie et al., 2016), with the extreme value of 1590 W/m^2 in the densest part of Tokyo at the peak of air-conditioning demand (Ichinose et al., 1999). In regard to their effects, the researchers found that AH fluxes can cause urban air temperatures to increase by several degrees (Fan and Sailor, 2005; Ferguson and Woodbury, 2007; Chen et al., 2009; Zhu et al., 2010; Feng et al., 2012; 2014; Menberg et al., 2013; Wu and Yang, 2013; Bohnenstengel et al., 2014; Chen et al., 2014a; Yu et al., 2014; Xie et al., 2016), induce the atmosphere more turbulent and unstable, change the urban heat island circulation, strengthen the air vertical movement (Ichinose et al., 1999; Block et al., 2004; Fan and Sailor, 2005; Chen et al., 2009; Feng et al., 2012; 2014; Bohnenstengel et al., 2014; Yu et al., 2014; Xie et al., 2016), enhance the convergence of water vapor in cities, and change the regional precipitation patterns (Feng et al., 2012; 2014; Xie et al., 2016). In spite that meteorology conditions and air quality are inextricably linked, however, few investigations have paid attention to how the air quality is altered by the changes of regional meteorology induced by anthropogenic heat. The results from the limited studies have showed that this impact is significant in and around large urban areas and should be considered in the air pollution predictions (Ryu et al., 2013; Yu et al., 2014; Xie et al., 2016).

Over the past decades, South China has been suffering the air quality deterioration (Wang et al., 2007; 2009b; Chan and Yao, 2008; Liu et al., 2013b), with high ozone (O_3) or poor visibility frequently occurring in urban areas (Wang et al., 2007; Fang et al., 2009) and the background air pollutant concentrations steadily increasing (Wang et al., 2009a; Liu et al., 2013b). South China generally refers to Guangdong, Guangxi, Hainan, Hong Kong, and Macau. The main feature of the terrain is mountainous and hilly. The majority of South China has a humid subtropical climate. Winters are mild, while summers are hot and muggy. It faces the South China Sea to the south, and has the longest coastline in China. So there are many islands in South China, including Hainan Island. These coastal areas can be influenced by both the monsoon and the dreaded typhoon. The air pollutions in South China may be related with the rapid urban expansion, especially in the Pearl River Delta (PRD) region. The PRD region consists of nine cities in Guangdong Province (Guangzhou, Shenzhen, Zhuhai, Dongguan, Zhongshan, Foshan, Jiangmen, Huizhou and Zhaoqing) plus Hong Kong and Macau (shown in the green square of Fig. 1b). As the most urbanized and industrialized part of South China, PRD has become the largest metropolitan area in the world within a very short time (Word Bank Group, 2015). Thus, many previous studies have tried to figure out the effects of urbanization on urban climate and air quality in this region (Lo et al., 2007; Wang et al., 2007; 2009b; Lu et al., 2010; Meng et al., 2011; Wu et al., 2011; Zhang et al., 2011; Feng et al., 2012; 2014; Chen et al., 2014b; Li et al., 2014; 2016). Among these studies, most researchers merely investigated how the expansion of urban land-use influences the meteorology processes (Lo et al., 2007; Wang et al., 2007; 2009b; Lu et al., 2010; Meng et al., 2011; Wu et al., 2011; Feng et al., 2012; Chen et al. 2014b; Li et al., 2016). Some also linked these changes of meteorological factors with the regional air quality, and quantified the impacts of land-use changing on air pollution (Wang et al., 2007; 2009b; Feng et al., 2012; Chen et al., 2014b; Li et al., 2014; 2016). Only a few researchers took AH into account (Meng et al., 2011; Feng et al., 2012; 2014). But they just clarified the impact of AH on meteorological conditions by merely adopting the fixed AH value in the urban parameterization scheme of meteorological models (Meng et al., 2011; Feng et al., 2012). Consequently, we still need to further understand how the excessive anthropogenic heat from urban expansion impacts on the severe air quality problems in this world famous region.

To fill the abovementioned knowledge gap, we present our new findings on the impact mechanism of anthropogenic heat on urban climate and regional air quality over South China in this paper, including (1) the spatial and temporal characteristics of AH emissions in South China, (2) how to implement the inhomogeneous AH data into the air quality model WRF/Chem, (3) the impacts of AH fluxes on meteorological fields, and (4) the impacts of meteorology changes on the air quality in different cities over South China. Detailed descriptions about the estimating method for anthropogenic heat emissions, the adopted WRF/Chem model with special configurations, and the observation data for model validation are presented in Sect. 2. Main results, including the inhomogeneous distribution of AH, the model evaluation, and the three-dimensional changes of meteorological fields and air pollutant concentrations are presented in Sect. 3. The summary is given in Sect. 4.

2. Methodology and data

2.1 Method for estimating anthropogenic heat fluxes

The top-down energy inventory method, which predicts AH emissions based on the statistics data of energy consumption, is the most common approach and widely used all over the world (Sailor and Lu, 2004; Flanner, 2009; Hamilton et al., 2009; Lee et al., 2009; Allen et al., 2011; Iamarino et al., 2012; Quah and Roth, 2012; Chen et al., 2014a) as well as in China (Chen et al., 2012; Xie et al., 2015; 2016; Lu et al., 2016). On basis of the previous studies, AH fluxes over the area between (101°E, 16°N) and (119°E, 26°N) in 1990, 1995, 2000, 2005, 2010 and 2014 are calculated in this study by the following equation:

$$Q_F = Q_{F,I} + Q_{F,B} + Q_{F,V} + Q_{F,HM} \quad (1)$$

where, Q_F is the total anthropogenic heat flux (W/m^2); $Q_{F,I}$, $Q_{F,B}$, $Q_{F,V}$, and $Q_{F,HM}$ represent the heat emitted from the industry sector, buildings, vehicles and human metabolism (W/m^2), respectively. To accurate estimate the spatial heterogeneity of AH fluxes, the estimated area is gridded as 456 rows and 264 columns with the grid spacing of 2.5 arcmin. The heat flux generated by human metabolism at each grid is estimated as:

$$Q_{F,HM} = P \cdot (M_d \cdot h_d + M_n \cdot h_n) / h \quad (2)$$

where, P is the population number at a grid. h_d, h_n and h are the hours of daytime, nighttime and a whole day. In this study, they are set to be 16, 8 and 24, respectively. M_d and M_n are the average human metabolic rate (W/person) during the daytime and at night. Referring to the previous studies (Sailor and Lu, 2004; Chen et al., 2012; Quah and Roth, 2012; Xie et al., 2015; 2016; Lu et al., 2016), we determined that the metabolic rate of a typical man is 175 W for the active daytime (M_d) and 75 W for the sleep period (M_n).

Based on the work of Flanner (2009), Lu et al. (2016) and Xie et al. (2016), it is reasonably assumed that all non-renewable primary energy consumption used for human activities is thermally dissipated as AH. So, $Q_{F,I}$, $Q_{F,B}$, and $Q_{F,V}$ at each grid can be estimated by using the data of non-renewable energy consumption (coal, petroleum, natural gas, and electricity etc.) from different categories. The amount of AH fluxes for one category can be estimated by the following equation:

$$Q_x = \eta \cdot \varepsilon \cdot C / (t \cdot A) \quad (3)$$

where, Q_x represents $Q_{F,I}$, $Q_{F,B}$ or $Q_{F,V}$. C is the primary energy consumption from a category at a grid (metric ton standard coal). ε is the calorific value of standard coal equivalent, with the recommended value of 29.271×10^3 kJ/kg (Chen et al., 2012; Lu et al., 2016; Xie et al., 2015;

2016). η is the efficiency of heat release, with the typical value of 60% for electricity or heat-supply sector and 100% for other sectors (Lu et al., 2016; Xie et al., 2016). t is the time duration of used data, which is set to be 31536000 s (seconds in a year) in this study. A represents the area of a grid (km^2). To quantify the value of C for each grid, we first of all obtain the energy consumption data from 1990 to 2014 in China Energy Statistical Yearbooks. Then we double check and modify the data in typical cities on basis of the Yearbooks in Guangdong, Guangxi, Hainan province and Hong Kong. In the end, the total numbers are apportioned according to the value of gross domestic product (GDP) or population density at each grid. GDP is used for industry and vehicle, while population is chosen for building. The population density with the resolution of 2.5 arcmin in 1990, 1995, 2000, 2005 and 2010 can be downloaded from Columbia University's Socioeconomic Data and Applications Center. The gridded GDP data are developed and applied based on the work of Liu et al. (2013a). The spatial distributions of GDP and population in 2014 are unobtainable, and thereby the data in 2010 are used as the surrogates.

2.2 WRF/Chem and its configuration

The WRF/Chem version 3.5 is applied to investigate the impacts of AH fluxes on regional meteorology and air quality over South China. WRF/Chem is a new generation of air quality modeling system, in which the feedbacks between meteorology and air pollutants are included by fully coupling the meteorological model (WRF) with the chemical modules (Chem). WRF/Chem has been widely used in simulating air quality in China and proved to be a reliable modeling tool from city-scale to meso-scale (Wang et al., 2009b; Liu et al., 2013b; Yu et al., 2014; Liao et al., 2015; Xie et al., 2016).

Three simulations are conducted in this study. One does not take the contribution of AH into account while the other two incorporate WRF/Chem with the fixed or the inhomogeneous AH fluxes (The details are presented in Sect. 2.3). Except for the setting of AH parameterization, other configurations (such as the physical schemes, the chemical schemes and the emission inventories etc.) for all simulations are the same. Thus, the difference between the modeling results can illustrate the effects of AH. As shown in Fig. 1, two nested domains are used. The outermost domain (Domain 1, D01) has the horizontal grids of 121×95, with the grid spacing of 27km. The second domain (Domain 2, D02) covers Guangdong, Guangxi, and Hainan provinces, with the center point at (110.4°E, 20.9°N), the horizontal grids of 192×105, and the grid spacing of 9km. For all domains, from the ground level to the top pressure of 100hPa, there are 31 vertical sigma layers with about 10 in the planetary boundary layer (PBL). In South China, January is generally representative of the relatively cold and dry season, while July represents the relatively hot and wet weather condition (Wang et al., 2014). Thus, January and July of 2014 are chosen for simulations and analysis in this study.

The detailed options for the physical and chemical parameterization schemes used in this study are shown in Table 1. Additionally, a Single Layer Urban Canopy Model (SLUCM) coupled in Noah Land Surface Model (Noah/LSM) is adopted for better modeling the urban effects.

Following the work of Liu et al. (2013b) and Wang et al. (2014), the default values for urban canopy parameters in SLUCM are substituted by the typical values in South China. As shown in Table 2, the values for building height, roof width, road with, urban fraction, and surface albedo are modified for the cities in and outside PRD, respectively. The recently updated Moderate Resolution Imaging Spectroradiometer (MODIS) land-use data (20 categories) with 30 arc seconds grid spacing are used to replace the default USGS (U.S. Geological Survey) land-use data in WRF/Chem, because the USGS data are too outdated to illustrate the intensive urbanization over South China. For chemistry, the RADM2 gas-phase chemistry scheme and the MADE/SORGAM aerosol scheme are adopted. RADM2 (Regional Acid Deposition Model version 2) contains 63 prognostic species and 136 reactions (Balzarini et al., 2015). MADE/SORGAM is the classical aerosol module used in WRF/Chem (Grell et al., 2005), where the Aerosol Dynamics Model for Europe (MADE) (Ackermann et al., 1998) contains the Secondary Organic Aerosol Model (SORGAM) (Schell et al., 2001). The anthropogenic emissions are mainly from the 2012-year Multi-resolution Emission Inventory for China (MEIC) with 0.25° grid spacing. This MEIC inventory based on RADM2 mechanism is re-projected for the grids of China in both domains. For the grids outside of China, the inventory developed by Zhang et al. (2009b) is used. The biomass burning emissions are acquired from the work of Li et al. (2016). The biogenic emissions are calculated online by using MEGAN2.04 (Guenther et al., 2006). The NCEP global reanalysis data with the grid spacing of 1° and 27 vertical levels are selected to provide the initial meteorological fields and boundary conditions. The initial chemical state and boundary conditions are obtained from the modeling results from the global chemistry transport model MOZART-4.

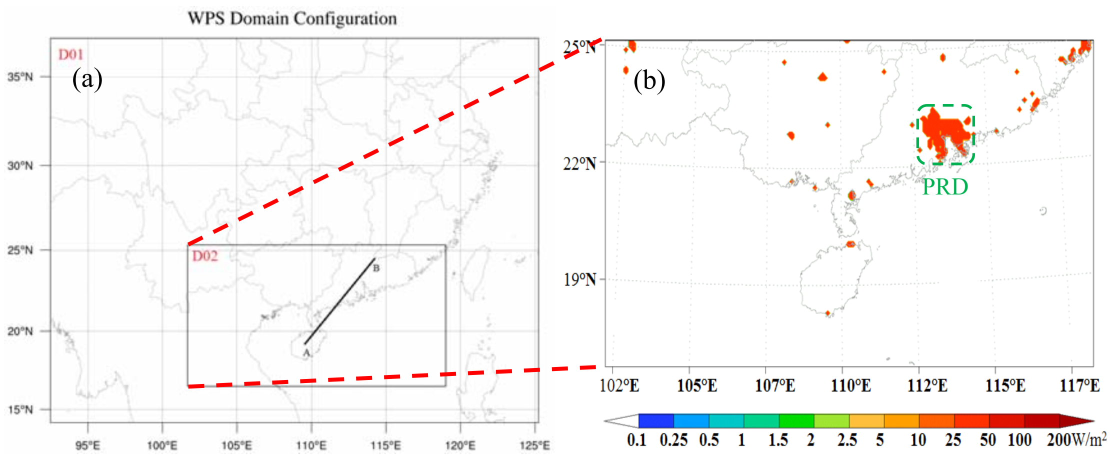

Fig. 1. WRF/Chem domain configuration, including (a) two domains for simulations and (b) enlarged view of domain 2 with fixed AH value of 50 W/m^2 for all urban grids used in the simulation case Fix_AH . Line AB in (a) denotes the location of the vertical cross section used in Fig. 4, Fig. 6, Fig. 8, Fig. 9, and Fig. 10. The green square in (b) presents the location of the Pearl River Delta (PRD) region.

Table 1. The grid settings, physics and chemistry options for all simulations

Items	Contents
Dimensions (x,y)	(121,95), (192,105)
Grid size (km)	27, 9
Time step (s)	150
Microphysics	Purdue Lin microphysics scheme (Lin et al., 1983)
Long-wave radiation	RRTM scheme (Mlawer et al., 1997)
Short-wave radiation	Goddard scheme (Kim and Wang, 2011)
Cumulus parameterization	Grell 3D (Grell and Devenyi, 2002)
Surface layer	Eta similarity (Janjic, 1994)
Land surface	Noah land surface model (Chen and Dudhia, 2001)
Planetary boundary layer	Mellor-Yamada-Janjic scheme (Janjic, 1994)
Gas-phase chemistry	RADM2 (Stockwell et al., 1990)
Photolysis scheme	Madronich photolysis (Madronich, 1987)
Aerosol module	MADE (Ackermann et al., 1998) / SORGAM (Schell et al., 2001)

Table 2. The modified values of main urban canopy parameters for the PRD region and other cities.

Parameter	Unit	PRD	Other cities
Building heigh	m	20	10
Roof width	m	15	10
Road width	m	10	10
Urban fraction	Fraction	0.95	0.9
Surface albedo of roof	Fraction	0.2	0.2
Surface albedo of wall	Fraction	0.2	0.2
Surface albedo of road	Fraction	0.2	0.2
roughness length for momentum over roof	m	0.15	0.15
roughness length for momentum over wall	m	0.05	0.05
roughness length for momentum over road	m	0.05	0.05

2.3 The configurations for AH parameterization

As shown in Table 3, three cases of numerical experiments are performed to evaluate the effects of AH. Non_AH is the base case, which does not consider the effects of AH. In Fix_AH, the default option for AH in SLUCM of WRF/Chem is adopted. For Grd_AH, we modify the AH parameterization, and the gridded AH flux data estimated in Sect. 2.1 are used to simulation the spatial heterogeneous effects of AH on meteorology and air quality. The difference between the modeling results of Fix_AH and Grd_AH can illustrate the model improvement caused by considering the spatial heterogeneity of AH. Comparing the results from Non_AH and Grd_AH, we can finally demonstrate the exact impacts of anthropogenic heat.

Table 3. Three simulations conducted in this study

Cases	Description
Non_AH	excluding anthropogenic heat emissions in SLUCM
Fix_AH	including anthropogenic heat emissions in SLUCM, but using the default AH option with fixed value 50 W/m^2 for all urban grids
Grd_AH	including anthropogenic heat emissions in SLUCM, and using the inhomogeneous AH emissions in 2014 estimated in Sect. 2.1

In SLUCM of WRF/Chem, the AH for one grid is determined by the fixed AH value, the fixed temporal diurnal pattern, and the urban fraction value (Chen et al., 2011; Yu et al., 2014; Xie et al., 2016). This default parameterization for AH can be described by the following algorithm:

$$SH = F_V \cdot SH_V + F_U \cdot (SH_U + AH_{fixed}) \quad (4)$$

where SH is the total sensible heat flux in a grid. F_V and SH_V are the fractional coverage and the sensible heat flux of vegetations, respectively. F_U and SH_U are those of urban surfaces. AH_{fixed} represents the fixed AH value for all urban areas (Chen et al., 2011). With respect to Grd_AH, we modify Eq. 4 by incorporating the inhomogeneous AH data (Q_F) as follow:

$$SH = F_V \cdot SH_V + F_U \cdot (SH_U + Q_F) \quad (5)$$

The gridded AH fluxes in 2014 from Sect. 2.1 (with the grid spacing of about 4km) are re-projected to domain 2 (9km) by the coordinates of each grid. To account for temporal variability, the diurnal variation pattern recommended for PRD by Zheng et al. (2009) and Lu et al. (2016) is adopted. It was reported that there is no significant seasonal difference in heating over South China (Lu et al., 2016). Thus, the monthly variation of AH is not considered in this study.

2.4 Method for model evaluation

The observation data of meteorology factors and air pollutants in Guangzhou, Shenzhen, Nanning and Haikou are used to validate the WRF/Chem simulations in this study. The hourly observation records of 2-m temperature, 10-m wind speed and 2-m relative humidity in January and July of 2014 can be obtained from the National Meteorological center of China Meteorological Administration. The relevant time series of PM_{10} and O_3 concentrations can be acquired from China National Environmental Monitoring Center. The assurance/quality control (QA/QC) procedures for these data strictly follow the national standards. As described by Liao et al. (2015) and Xie et al. (2016), the mean bias (MB), root mean square error (RMSE) and correlation coefficient (COR) between observation records and modeling results are used to evaluate the model performance.

3. Results and discussions

3.1 Spatial distribution of AH fluxes in South China

Fig. 2 shows the spatial distribution of AH in 1990, 1995, 2000, 2005, 2010 and 2014 over South China. Obviously, big cities especially the cities in PRD have the largest values from the 1990s till now. In 1990, except for those in Guangdong and Hong Kong, the AH fluxes in most areas of South China are less than 2 W/m^2. From 1995 to 2000, the AH fluxes in most parts of PRD (except for those in Hong Kong) are less than 5 W/m^2, and those in other areas of South China are generally lower than 2.5 W/m^2. After 2005, however, the AH fluxes exceed 10 W/m^2 in many cities of South China, with the high values over 50 W/m^2 in and around Hong Kong. For the annual mean AH flux over the whole administrative district of different province, the value in Guangdong continuously increases from 0.30 W/m^2 for 1990 to 1.68 W/m^2 for 2014, while the heat release in Guangxi and Hainan keeps in a low level (< 0.5 W/m^2) but with an obvious increasing. The annual mean AH values in the downtown areas are much higher than the regional ones. For instance, the PRD city cluster always has the highest anthropogenic heat emissions in South China. As shown in Table 4, the annual mean value in the built-up areas aggrandizes from 5.1 W/m^2 in 1990 to 58 W/m^2 in 2014. These results are similar to those reported by Chen et al. (2012; 2014a) and Xie et al. (2015), and the temporal variation pattern also fits in well with the economic boom over South China in the past decades.

In 2014, as illustrated in Fig. 2f, most important cities in South China have the AH fluxes more than 5 W/m^2. High fluxes generally occur in Guangdong province, especially in the PRD region and the Chao-Shan area, with the typical values over 10 W/m^2. In the build-up area of Guangzhou, the AH fluxes are close to 60 W/m^2, which are similar to those in Seoul of Korea (Lee et al., 2009), Toulouse of France (Pigeon et al., 2007), and some US cities (Sailor and Lu, 2004; Fan and Sailor, 2005). The regional highest value occurs in Hong Kong, with the value exceeding 100 W/m^2. This value is comparable to those in the most crowded megacities, such as Shanghai (Xie et al., 2016), Tokyo (Ichinose et al., 1999), London (Hamilton et al. 2009; Iamarino et al. 2012), and Singapore (Quah and Roth, 2012). In Nanning and Haikou, the annual mean AH fluxes over the whole administrative district are close to 10 W/m^2. These results can also be supported by other previous investigations (Flanner, 2009; Chen et al., 2012; 2014a; Xie et al., 2015; Lu et al., 2016). With regard to the default AH option in WRF/Chem, the fixed value of 50 W/m^2 is usually used for all urban grids (shown in Fig. 1b). Compared with this unrealistic distribution pattern (Fig. 1b), our spatial distribution of AH based on the population (Fig. 2f) reflects the heterogeneity of economic activities in South China, suggesting that our method is effective and the results are reasonable. So, our AH data can be used in models to investigate their impacts on urban climate and air quality.

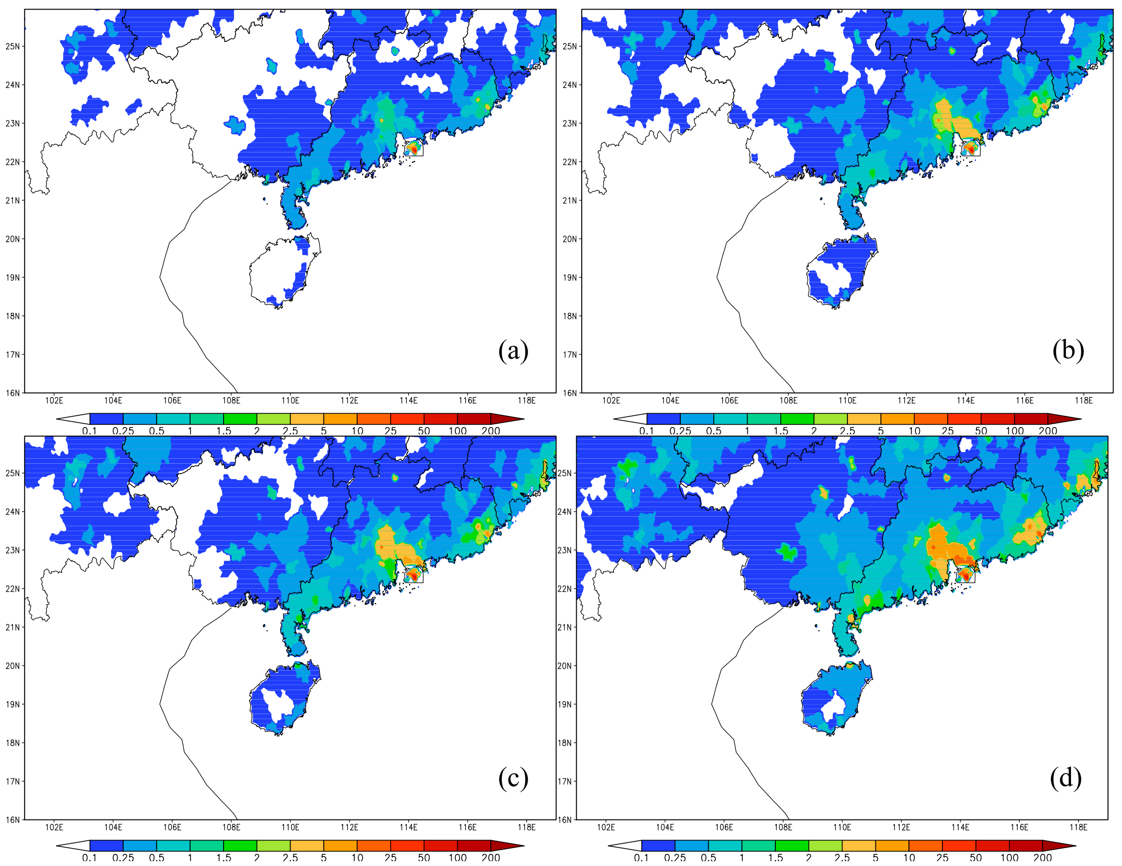

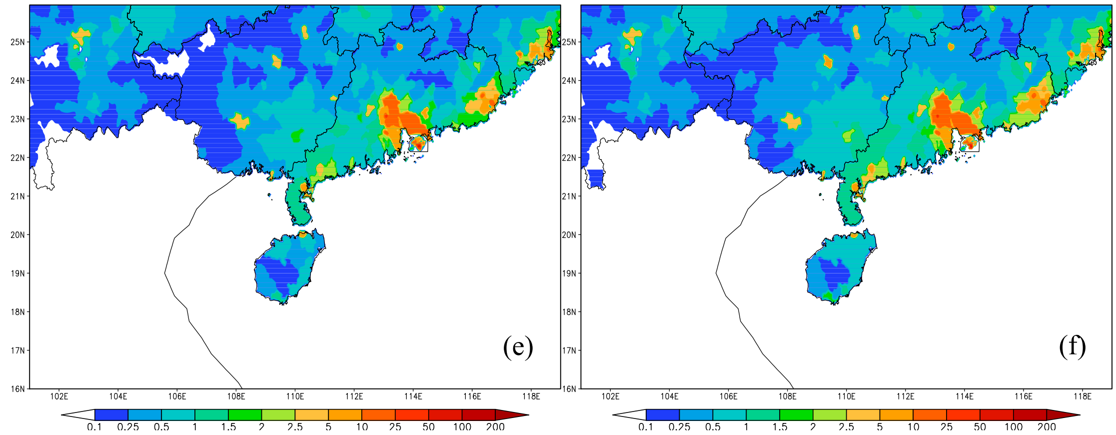

Fig. 2. Annual-mean anthropogenic heat fluxes between (101°E, 16°N) and (119°E, 26°N) with the resolution of 2.5 arcmin in 1990 (a), 1995 (b), 2000 (c), 2005 (d), 2010 (e) and 2014 (f), respectively.

Table 4 Annual average anthropogenic heat flux in different administrative district over South China (W/m^2)

Province		This study					
		1990	1995	2000	2005	2010	2014
Guangdong	Regional [a]	0.30	0.48	0.61	1.05	1.53	1.68
	Urban area in PRD	5.11	11.13	14.51	30.82	49.41	58.03
Guangxi	Regional [a]	0.11	0.16	0.17	0.26	0.38	0.44
Hainan	Regional [a]	0.04	0.09	0.14	0.23	0.37	0.49

[a] Regional represents the average value over the whole area of a province

3.2 Simulation performance

To evaluate the model performance and clarify the better AH parameterization, the modeling results from Fix_AH and Grd_AH are compared with the observation data in two typical months (January and July). Table 5 presents the performance statistics, including the values of monthly mean (Mean), mean bias (MB), root mean squared error (RMSE) and correlative coefficient (COR), which are all quantified for 2-m temperature (T_2), 2-m relative humidity (RH_2), 10-m wind speed (WS_{10}), ozone (O_3), and particles (PM_{10}) in Guangzhou (GZ), Shenzhen (SZ), Nanning (NN), and Haikou (HK).

As shown in Table 5, the correlation coefficients (COR) between observations and simulations at four sites are generally about 0.80 for T_2, over 0.75 for RH_2, and close to 0.70 for WS_{10} in both January and July (statistically significant at the 95 % confident level). So adding AH in WRF/Chem (Fix_AH and Grd_AH) can well describe the urban meteorological conditions in the typical cities over South China. Compared with the observation records of T_2, except for Shenzhen in January, both Fix_AH and Grd_AH tend to slightly simulate higher 2-m air temperature at four sites in both months, which can be attributed to the uncertainty of urban canopy and surface parameters (Liao et al., 2015; Xie et al., 2016). These overestimates are acceptable because the MB values are smaller than 1.8 ℃ in January and smaller than 0.8 ℃ in July. Moreover, when the gridded AH fluxes are taken into account (Grd_AH), the modeling results of air temperature can be improved, with the mean bias (MB) decreasing by 0.1 - 0.3 ℃

and the correlation coefficient (COR) increasing by 0.02 - 0.05 (from Fix_AH to Grd_AH). With regards to RH_2, the modeling values from two simulations (Fix_AH and Grd_AH) are close to the observations. The best simulation occurs in Haikou, and the results at the other three sites are reasonable as well, only with the bias within ±10%. These 2-m relative humidity predictions can be improved from Fix_AH to Grd_AH. When we consider the heterogeneity of AH fluxes in Grd_AH, the values of MB and RMSE are closer to 0 and those of COR are closer to 1. For WS_{10}, because the modeling near-surface wind speed is generally influenced by local underlying surface characteristics more than other meteorological parameters (Liao et al., 2015; Xie et al., 2016), both Fix_AH and Grd_AH slightly overvalue the 10-m wind speed at four sites. In case Fix_AH, the MB for WS_{10} is generally around 1m/s in both months, and the RMSE is less than 2.6 m/s in January and around 2m/s in July. However, the predictions are obviously improved in case Grd_AH. The MB decreases to 0.4-0.9 m/s in January and 0.4-0.7 m/s in July, and the values of COR also increase from 0.68 (Fix_AH) to 0.74 (Grd_AH) in July. These improvements from Fix_AH to Grd_AH for T_2, RH_2 and WS_{10} predictions suggest that the default value of WRF/Chem for all urban grids overestimates the AH fluxes in these cities, and our gridded AH data as well as the new parameterization scheme can exactly catch the heterogeneity of the heat released from the metropolitans of South China.

Table 5 also illustrates the performance of WRF/Chem simulations for the main air pollutants (O_3 and PM_{10}). Obviously, both Fix_AH and Grd_AH can capture the magnitude and temporal variation of main air pollutants in these typical cities over South China, and the simulation with gridded AH fluxes (Grd_AH) can provide better predictions. For Grd_AH, the correlation coefficients (COR) for PM_{10} in all cities are around 0.62 in January and around 0.65 in July (statistically significant at the 95 % confident level). The MB values for PM_{10} are only -0.4 - 1.0 $\mu g/m^3$ in January and 1.8 -3.1 $\mu g/m^3$ in July. With respect to O_3, the values of MB are -9.2 - -16.1 ppb in January and -10.0 - -13.5 ppb in July. These underestimates should be related with the increasing of WS_{10} and the rising of PBL caused by positive biases in T_2. The uncertainties in emissions of ozone precursors (NO_x and VOCs) may cause these biases as well (Liao et al., 2015; Xie et al., 2016). However, the values of COR for O_3 are 0.60 - 0.71 in January and 0.60 - 0.64 in July (statistically significant at the 95 % confident level), proving that these modeling results are reasonable and acceptable.

Fig. 3 presents the monthly-averaged differences of O_3 and PM_{10} between Fix_AH and Grd_AH (Fix_AH minus Grd_AH) at the surface layer over the modeling domain 2 (D02). Obviously, there are some differences between the two simulations that use different AH parameterizations. These differences are more obvious in and around big cities because the AH are related with the human activities. Moreover, the differences in January are higher than those in July, implying that the adding of AH can arouse more atmospheric disturbances in winter. From this point of view, Grd_AH can better describe the spatial and temporal heterogeneity of the impacts of AH on regional air quality.

Table 5 Summary of statistics for comparison between simulated and observed hourly averaged meteorological and chemical data in four cities of South China

Case		Fix_AH										Grd_AH									
		January					July					January					July				
Vars[a]	Site[b]	Mean[c]		MB	RMSE	COR[f]	Mean[c]		MB	RMSE	COR[f]	Mean[c]		MB	RMSE	COR[f]	Mean[c]		MB	RMSE	COR[f]
		SIM[d]	OBS[e]				SIM[d]	OBS[e]				SIM[d]	OBS[e]				SIM[d]	OBS[e]			
T_2 (℃)	GZ	14.0	12.2	1.8	3.1	0.75	29.0	28.4	0.6	4.0	0.72	13.8	12.2	1.6	2.9	0.78	28.8	28.4	0.4	2.1	0.76
	HK	18.9	17.3	1.6	2.0	0.79	29.0	28.4	0.6	1.7	0.79	18.5	17.3	1.3	1.8	0.81	28.9	28.4	0.5	1.6	0.83
	NN	13.9	12.2	1.7	2.9	0.84	28.0	27.7	0.3	2.5	0.77	13.7	12.2	1.4	2.7	0.86	27.9	27.7	0.2	2.0	0.81
	SZ	14.6	14.7	-0.1	1.8	0.84	29.9	29.1	0.8	2.0	0.76	14.4	14.7	-0.3	1.9	0.86	29.6	29.1	0.5	1.9	0.81
RH_2 (%)	GZ	64.2	73.5	-9.3	18.5	0.74	68.4	78.8	-10.4	17.9	0.73	66.8	73.5	-6.7	16.8	0.75	71.3	78.8	-7.5	16.8	0.76
	HK	75.6	78.2	-2.5	8.5	0.77	80.6	81.0	-0.3	7.8	0.80	77.0	78.2	-1.1	8.2	0.84	81.4	81.0	0.4	7.7	0.86
	NN	69.3	77.9	-8.6	18.2	0.74	87.7	83.5	4.2	8.8	0.79	72.3	77.9	-5.6	17.7	0.75	86.5	83.5	3.0	8.9	0.81
	SZ	65.9	63.3	2.6	11.7	0.75	74.2	78.0	-3.8	11.1	0.75	66.5	63.3	3.2	12.3	0.76	75.6	78.0	-2.4	10.5	0.83
WS_{10} (m/s)	GZ	3.1	2.4	0.7	1.9	0.75	2.6	1.8	0.8	1.8	0.68	2.8	2.4	0.4	1.3	0.76	2.4	1.8	0.6	1.4	0.74
	HK	4.3	3.3	1.0	2.3	0.74	3.6	2.7	0.9	1.7	0.68	4.2	3.3	0.9	1.8	0.76	3.2	2.7	0.5	1.4	0.74
	NN	2.5	1.3	1.2	2.3	0.73	2.3	1.5	0.8	2.1	0.68	2.0	1.3	0.7	1.5	0.75	1.9	1.5	0.4	1.2	0.74
	SZ	3.3	2.2	1.1	2.6	0.73	2.8	1.8	1.0	1.8	0.68	2.9	2.2	0.7	1.2	0.75	2.5	1.8	0.7	1.7	0.73
O_3 (ppb)	GZ	93.7	110.5	-16.8	66.6	0.55	42.2	57.0	-14.8	62.5	0.51	101.3	110.5	-9.2	68.3	0.68	45.3	57.0	-11.7	52.5	0.64
	HK	63.7	75.5	-11.8	48.7	0.58	15.4	25.3	-9.9	25.8	0.51	65.4	75.5	-10.1	48.2	0.71	15.3	25.3	-10.0	21.7	0.63
	NN	138.4	157.8	-19.4	85.4	0.54	33.8	48.9	-15.1	55.4	0.51	141.7	157.8	-16.1	79.5	0.62	35.4	48.9	-13.5	48.6	0.60
	SZ	64.7	80.0	-15.3	54.2	0.52	28.7	43.9	-15.5	50.1	0.52	67.3	80.0	-12.7	56.5	0.60	31.6	43.9	-12.3	41.0	0.61
PM_{10} (μg/m^3)	GZ	21.1	19.6	1.5	13.0	0.53	31.4	28.9	2.5	29.0	0.53	20.3	19.6	0.7	12.2	0.61	31.0	28.9	2.1	25.3	0.63
	HK	32.2	30.9	1.3	14.5	0.53	14.7	11.9	2.8	15.3	0.53	31.9	30.9	1.0	14.1	0.61	14.2	11.9	2.3	13.9	0.63
	NN	25.6	24.7	0.9	16.7	0.54	19.8	17.3	2.5	12.7	0.54	25.3	24.7	0.6	15.7	0.62	19.1	17.3	1.8	9.0	0.65
	SZ	27.7	28.4	-0.7	14.3	0.54	24.5	20.6	3.9	17.8	0.55	28.0	28.4	-0.4	13.4	0.62	23.7	20.6	3.1	14.3	0.66

[a] Vars indicates the variables, including temperature at 2m (T_2), relative humidity at 2m (RH_2), wind speed at 10m (WS_{10}), ozone (O_3) and PM_{10}; [b] Site indicates the city where the observation sites locate, including Guangzhou (GZ), Haikou (HK), Nanning (NN) and Shenzhen (SZ); [c] Mean indicates the monthly average value; [d] SIM indicates the simulation results from WRF/Chem; [e] OBS indicates the observation data; [f] COR indicates the correlation coefficients, with statistically significant at 95% confident level.

Above all, the WRF/Chem simulation accounting for the temporal and spatial distribution of AH (Grd_AH) has a relatively good capability in simulating urban climate and air quality over South China. So, the differences between the modeling results from Non_AH and Grd_AH can be used to quantify the impacts of anthropogenic heat on meteorology and air pollution.

3.3 Impacts of AH on meteorological conditions

Fig. 4a-d, Fig. 5a-d, Fig. 6a-b and Fig. 6g-h show the impacts of AH on surface meteorology, which are defined as the monthly-averaged differences of these meteorological factors between Grd_AH and Non_AH (Grd_AH minus Non_AH) at the surface layer over the modeling domain 2. Fig. 4e-f and Fig. 6c-f show the relevant vertical changes of the meteorological factors along the cross-section from (19.1°N, 108.9°E) to (24.8°N, 114.7°E) which is shown as the solid line AB in Fig. 1b. The vertical cross section analysis through the line AB is to discuss the different effects of AH on ambient environment between the big (Guangzhou) and the relatively small (Haikou) city.

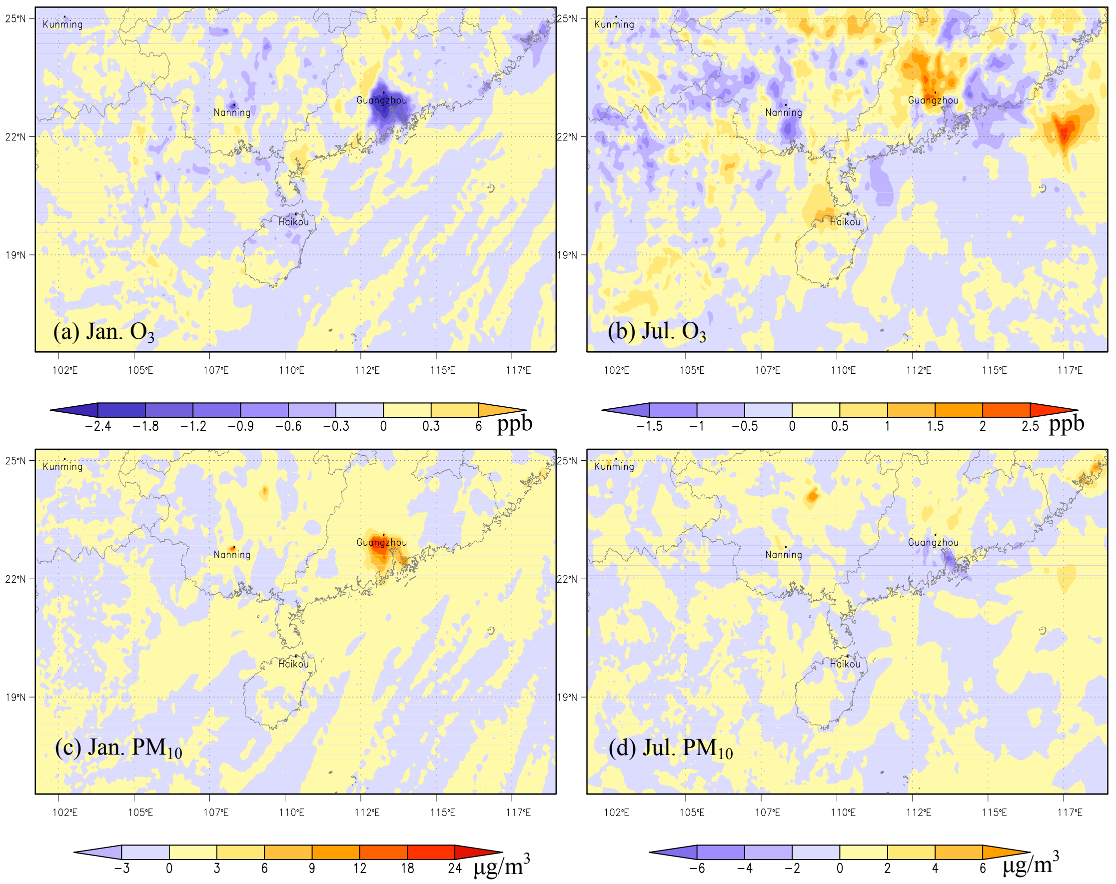

Fig. 3. The spatial distributions of monthly-averaged differences for surface O_3 and PM_{10} between Fix_AH and Grd_AH (Fix_AH minus Grd_AH). (a) and (c) show changes in January. (b) and (d) illustrate variations in July.

3.3.1 Changes of surface energy and air temperature

On account that AH and its diurnal variation are added to the sensible heat item in

WRF/Chem, the adding of gridded AH fluxes should increase the modeling results of sensible heat fluxes (SHF) over South China. As shown in Fig. 4a and b, the spatial patterns of SHF changes in both January and July are similar to the spatial distribution of AH fluxes presented in Fig. 2f. The significant increments (> 10 W/m^2) of SHF over South China usually occur in and around mega-cities. Especially in the PRD city cluster, adding AH can cause SHF to increase by over 50 W/m^2 in both January and July.

For the 2-m air temperature (T_2) over South China, the AH fluxes can increase their values by adding more surface heat into the atmosphere. As presented in Fig. 4c and d, the patterns of the monthly-averaged T_2 changes are similar to those of SHF (Fig. 4a and b). In the urban areas, the adding of AH can lead to the significant increase of T_2, which may enhance the Urban Heat Islands (UHI). For example, the UHI intensity (the difference of monthly mean temperature between the maximum in urban areas and the minimum in surrounding rural areas) in PRD is about 1.7℃ in January and 1.3℃ in July for Non_AH case, while it increases to 2.4℃ in January and 1.8℃ in July for Grd_AH case. The maximum T_2 changes are usually found in the city centers of the PRD region, with the typical increments over 1.1 ℃ in January and over 0.5℃ in July. These findings are comparable to the values estimated for other cities (Fan and Sailor, 2005; Ferguson and Woodbury, 2007; Chen et al., 2009; Zhu et al., 2010; Menberg et al., 2013; Wu and Yang, 2013; Bohnenstengel et al., 2014; Yu et al., 2014; Xie et al., 2016), and can be confirmed by the similar researches in South China (Meng et al., 2011; Feng et al., 2012; 2014).

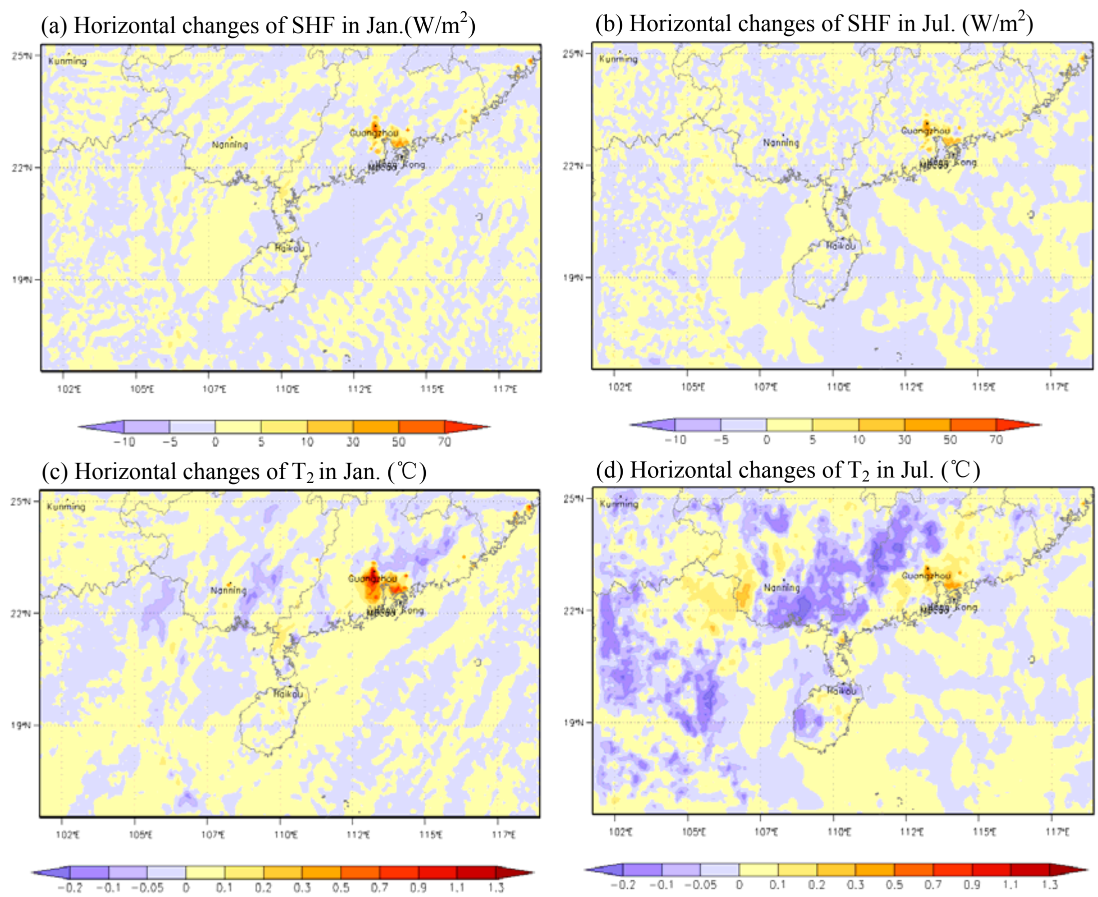

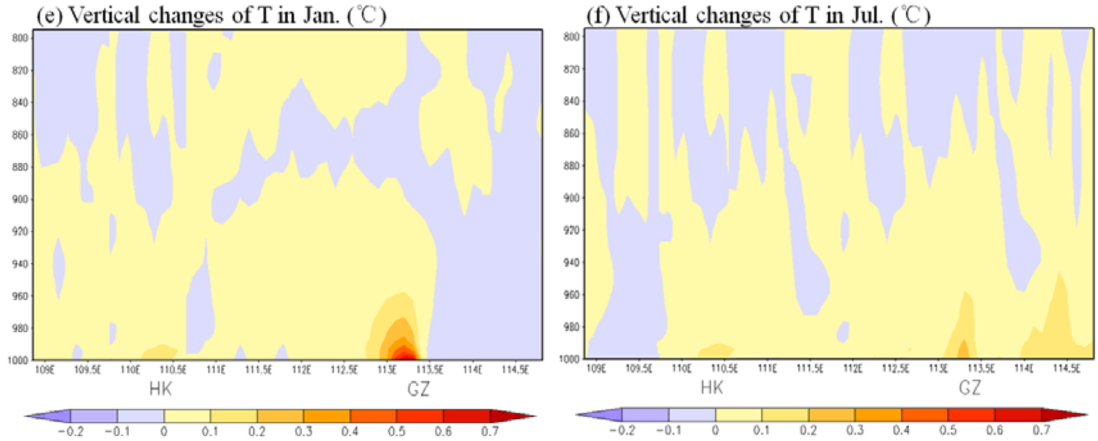

Fig. 4. The monthly-averaged differences between Grd_AH and Non_AH (Grd_AH minus Non_AH) for (a), (b) the spatial distribution of sensible heat flux (SHF); (c), (d) the spatial distribution of 2-m air temperature (T_2); (e), (f) the vertical distribution of air temperature (T) from the surface to the 800hPa layer along the line AB shown in Fig. 1b. Grd_AH and Non_AH represent the simulations with and without AH fluxes. (a), (c), and (e) show changes in January, while (b), (d), and (f) illustrate variations in July. In (e) and (f), HK and GZ are the abbreviations for Haikou and Guangzhou, respectively.

Fig. 4e and f present the vertical changes of air temperature from the surface to the 800hPa layer along the line AB (shown in Fig. 1b), and illustrate that the increases of air temperature causing by adding AH are mainly confined near the surface around the cities (Guangzhou and Haikou). These changes of air temperature in Guangzhou are more obvious than those in Haikou, because the AH emissions are much higher in Guangzhou. Furthermore, T_2 changes in winter (Fig. 4e) are more obvious than those in summer (Fig. 4f), with the monthly mean increment of T over 0.7℃ for January while only around 0.4℃ for July in Guangzhou. This phenomenon should be related with the fact that the background heat fluxes are much lower in winter so that the relative increase of T is more obvious.

3.3.2 Changes of boundary layer and wind field

The warming up of surface air temperature can enhance the vertical air movement in boundary layer (PBL), and thereby can increase the height of boundary layer (PBLH) as well. As shown in Fig. 5a and b, the boundary layer height becomes higher when the AH fluxes are taken into account. The big increments (more than 50m) usually occur in the urban areas of the PRD region. Because relative higher temperature increment in January can induce higher PBL in this cold season, the maximum changing values of PBLH can be 120m for January but only 90m for July.

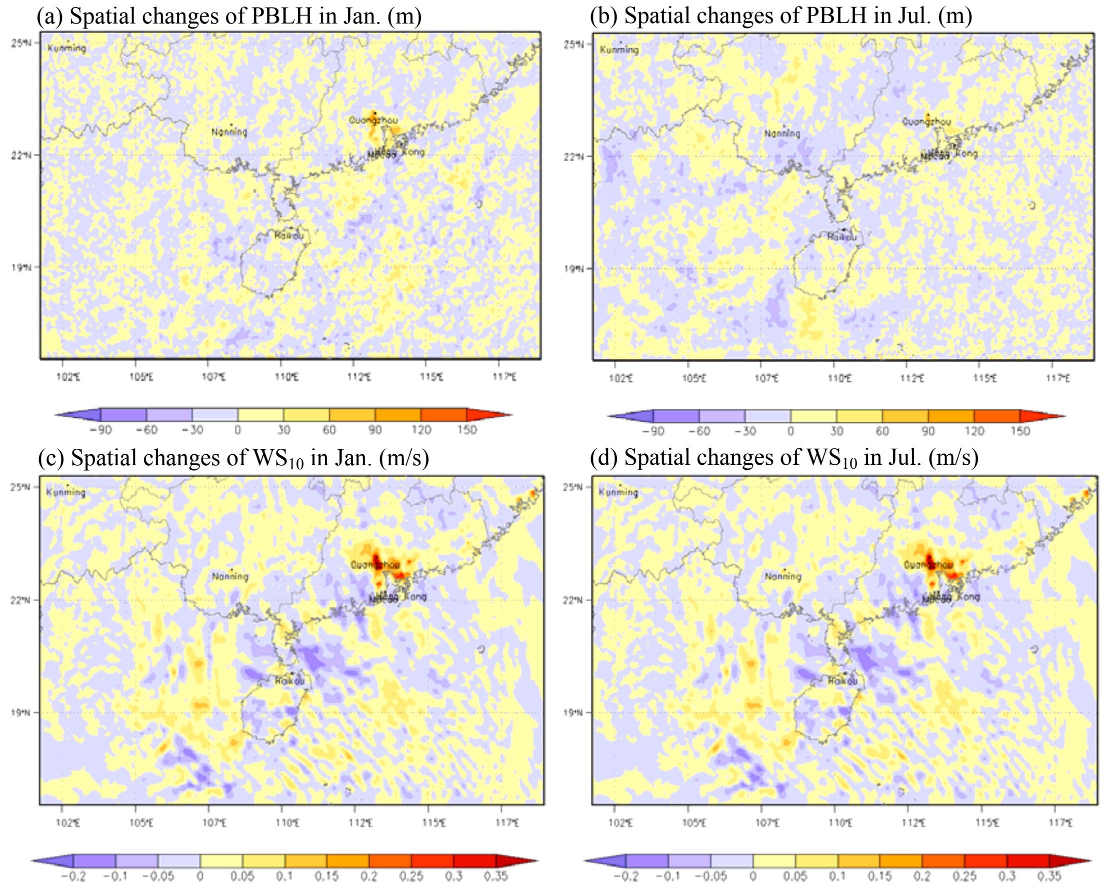

Fig. 5. The monthly-averaged differences of the height of planetary boundary layer (PBLH) and 10-m wind speed (WS_{10}) between Grd_AH and Non_AH (Grd_AH minus Non_AH). Grd_AH and Non_AH represent the simulations with and without AH fluxes. (a) and (c) show changes in January, while (b) and (d) illustrate variations in July.

Fig. 5c and d show the changes in the 10-m wind speed over South China. Obviously, adding AH can enhance the surface wind in the urban areas. The maximum increase is located in the PRD region, with the values over 0.35 m/s in January and 0.3 m/s in July. In other cities like Chaozhou, Nanning and Haikou, the increments are merely about 0.1 m/s. The warming of air temperature near surface as well as the rising of PBLH induced by adding AH in cities can generate an enhanced urban-breeze circulation. In previous studies, the increases in surface wind speed were considered to be related with this strengthened urban-breeze circulation (Chen et al., 2009; Ryu et al., 2013; Yu et al., 2014; Xie et al., 2016). Our results show that the vertical wind velocities above the Guangzhou and Haikou is enhanced in both January and July (Fig. 6c and d), and the simulated convergence at the surface near these cities increases by 0.04-0.13 /s in January and 0.05-0.18 /s in July (not shown). Consequently, we deduce that the enhanced vertical air movement causes the surface stronger convergence and thereby induces higher surface wind speed. It is worth mentioning that the changes of vertical air movement and surface wind may affect the local land-sea breeze circulation in the coastal cities. For example, AH emission in Haikou enhances the upward air movement above the city (Fig. 6c and d), causes the downward movement above the surrounding waters (Fig. 6c and d), and increases the surface wind from sea to land (stronger convergence). These changes imply that AH might strengthen sea breeze in the daytime and weaken land breeze at night.

3.3.3 Changes of moisture and rainfall

Fig. 6a and b presents the monthly-averaged differences of water vapor mixing ratio (VAPOR) at 2m between Grd_AH and Non_AH. Obviously, the air near the surface of cities becomes dryer. The negative centers occur in the PRD region, the Chao-Shan area, and some other cities, such as Haikou and Nanning. These cities are also the AH emission centers occurring in Fig. 2f. In the urban areas of PRD, the reductions of surface VAPOR can be -0.1 to -0.3 g/kg in January and -0.2 to -0.5 g/kg in July.

It was reported that the enhanced vertical air movement can transport more moisture from the surface to the upper layer, and thereby can modify the spatial and vertical distributions of moisture (Xie et al., 2016). This effect mechanism can be clearly illustrated by Fig. 6c-f in this study. As shown in Fig. 6c and d, the vertical wind velocities above Guangzhou and Haikou increase by the values of 0.2 – 0.5 cm/s in January and 0.5 - 1.0 cm/s in July, whereas w decreases in the rural areas with the reductions about -0.3m/s in January and over -0.5 cm/s in July. This pattern means that there are a strengthened upward air flow in cities and a strengthened downward air flow in the surrounding areas, implying that the adding of AH fluxes makes the atmosphere more unstable and tends to form deep convections in troposphere. So, as shown in Fig. 6e and f, more moisture can be transported from the surface to the upper layers. In Guangzhou, for example, the water vapor mixing ratios at the ground level decrease by -0.3g/kg in January and -0.5 g/kg in July, while those at the upper PBL increase by 0.1 g/kg in January and 0.3 g/kg in July. The impact of AH on water vapor is stronger in July. This seasonal difference can be ascribed to the facts that the atmosphere is more stagnant and dryer in winter and more convective and wetter in summer. Furthermore, the changes in Haikou are generally smaller than those in Guangzhou, which can be explained by the fact that the AH emissions are much lower in Haikou.

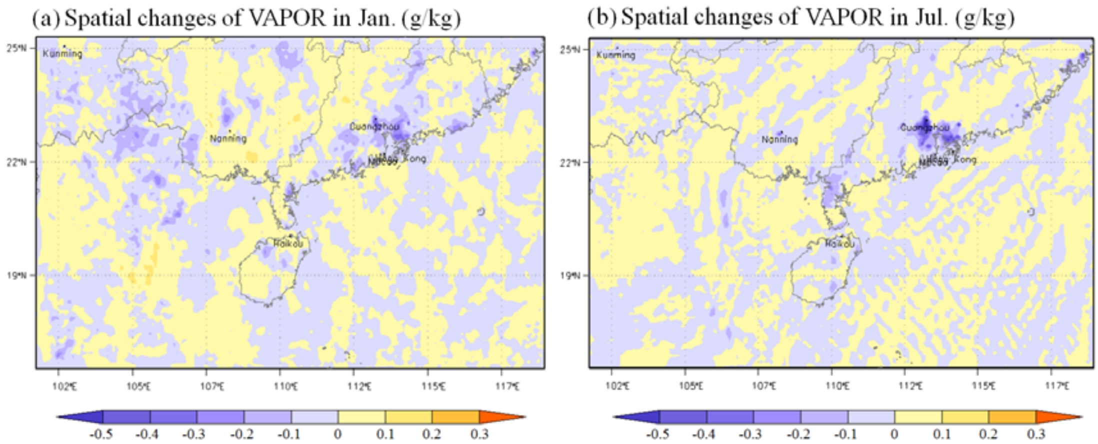

(c) Vertical changes of w in Jan. (cm/s)

(d) Vertical changes of w in Jul. (cm/s)

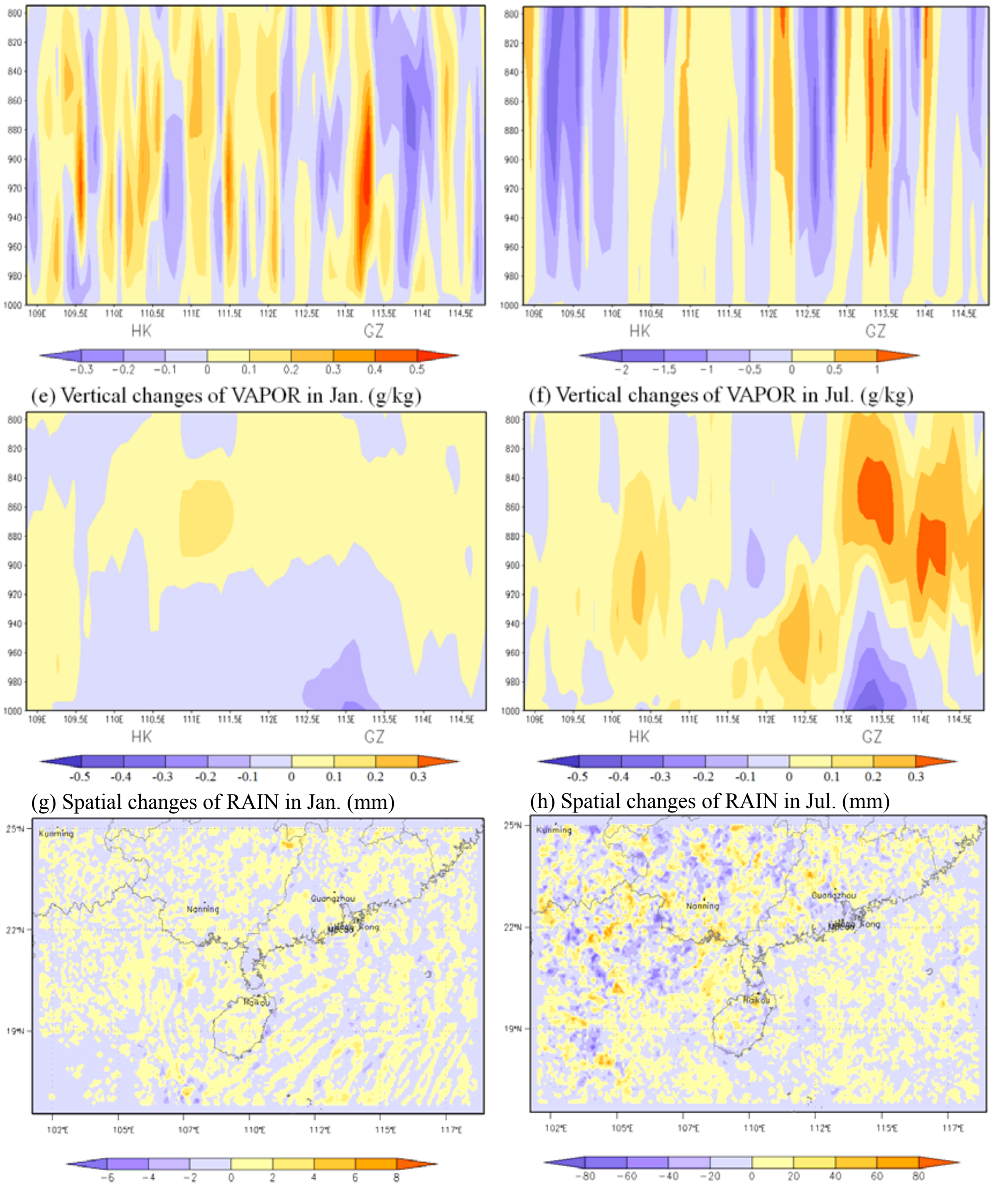

Fig. 6. The monthly-averaged differences between Grd_AH and Non_AH (Grd_AH minus Non_AH) for (a), (b) the spatial distribution of water vapor mixing ratio (VAPOR) at 2m; (c), (d) the vertical distribution of vertical wind velocity (w); (e), (f) the vertical distribution of VAPOR; (g), (h) the spatial distribution of precipitation (RAIN). The vertical cross section is from the surface to the 800hPa layer along the line AB shown in Fig. 1b. Grd_AH and Non_AH represent the simulations with and without AH fluxes. (a), (c), (e), and (g) show changes in January, while (b), (d), (f), and (g) illustrate variations in July. In (c), (d), (e), and (f), HK and GZ are the abbreviations for Haikou and Guangzhou, respectively.

More moisture transported from surface into the mid-troposphere can increase the precipitation in these urban areas as well. Fig. 6g and h illustrate the enhanced rainfall over South China both in January and July. Because of the negligible accumulative precipitation in winter, there are no significant differences between the Grd_AH and Non_AH simulations for rainfall in

January. But in July, the increment of rainfall can be more than 50mm in and around big cities. Moreover, according to the dominant southeast wind in summer, the moisture can be transported to the downwind areas of the PRD city cluster, which causes the increases of rainfall in the northwest part of Guangdong province with the maximum value over 80 mm.

3.3.4 Diurnal pattern of the changes

In order to better understand the different impacts of AH in the daytime and at night, the monthly-averaged diurnal variations of T_2, PBLH, and WS_{10} in January and July over the urban areas in Guangzhou are calculated based on the results from Grd_AH and Non_AH. As shown in Fig. 7a and b, adding AH fluxes can lead to an obvious increase of 2-m air temperature in both months, with the daily mean increase of 1.5℃ for January and 0.6 ℃ for July. The increment of T_2 at night in January (1.69℃) is larger than that in the daytime (1.31℃), whereas the changes during the whole day in July are all around 0.6℃, which suggests that AH can weaken the diurnal T_2 variation in winter. With respect to PBLH, the AH fluxes can also result in a higher boundary layer. In July (Fig. 7d), the increment of PBLH nearly keeps a constant value of 54m (4.7%) from morning till night. However, in January (Fig. 7c), the nighttime increase of PBLH is much higher than that in the daytime. This phenomenon may be related with the facts that the absolute PBLH values are lower and the air temperatures increase more in the winter nights. For WS_{10}, AH emission causes it to increase 0.07 m/s in January and 0.15m/s in July. Most increases occur in the daytime. The effect of AH on surface wind is negligible at night, which may be related to the fact that the land breeze at night (from land to sea) hinders the surface convergence (from sea to land) caused by AH.

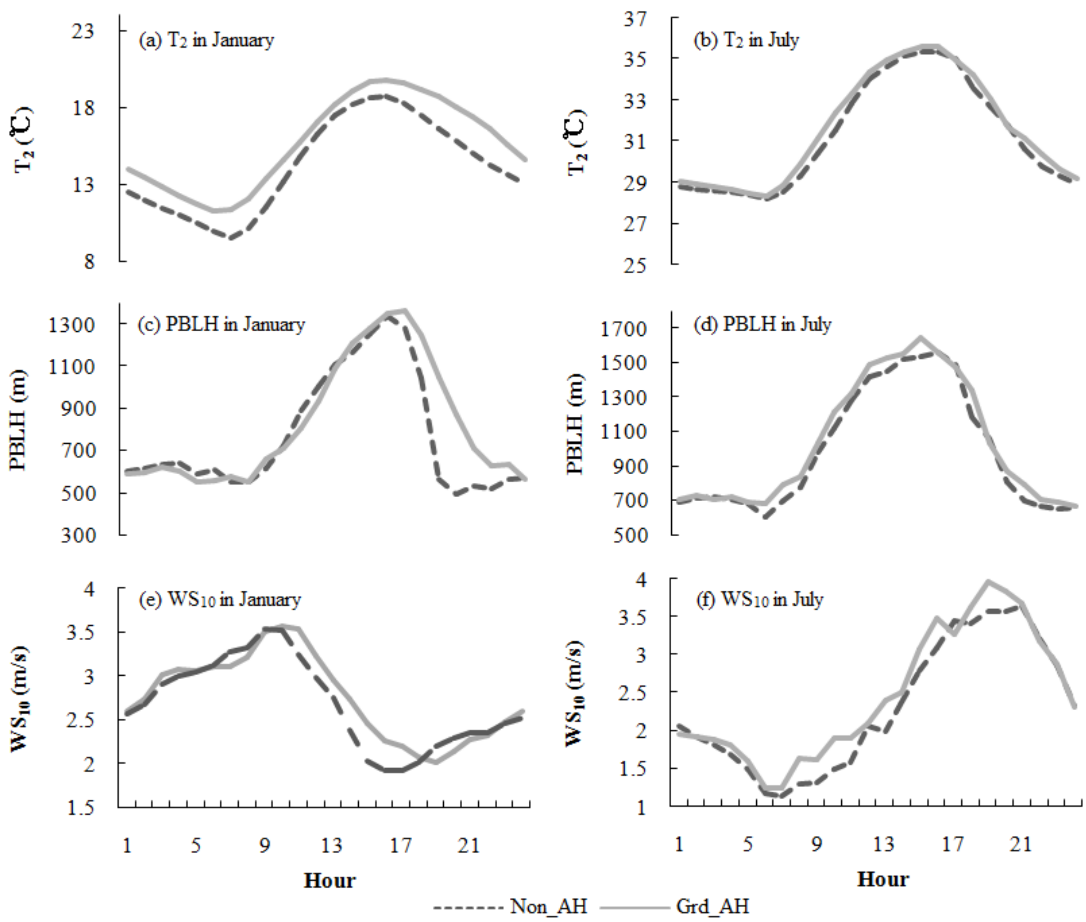

Fig. 7. The monthly-averaged diurnal variations for 2-m air temperature (T_2), the height of planetary boundary layer (PBLH), and 10-m wind speed (WS_{10}) over the urban areas in Guangzhou. Grd_AH and Non_AH represent the simulations with and without AH fluxes, respectively. (a), (c) and (e) show diurnal curves in January, while (b), (d) and (f) illustrate those in July.

3.4 Impacts of AH on main air pollutants

3.4.1 Changes of the spatial and vertical distribution of PM_{10}

Since adding AH changes the atmospheric conditions, it can affect the transportation and dispersion of air pollutants as well. Fig. 8a and b show the effects of AH on the spatial distribution of PM_{10} at the surface layer over South China in January and July. They illustrate that the concentrations of PM_{10} decrease in both season near the big cities, including the PRD city cluster, the Chao-shan area, and Nanning etc. The maximum reductions occur in the PRD region, with the monthly mean value over -10μg/m^3 for January and about -5μg/m^3 for July. Compared with the distribution of AH emissions as well as their effects on meteorological conditions, the main causes resulting in the reduction of surface PM_{10} should be attributed to the increase of PBLH, vertical upward air flow and surface wind speed, which can all facilitate PM_{10} transport and dispersion within the urban boundary layer. For another, as shown in Fig. 6h, the rainfall around the PRD cities can increase by 20-40% in July when the AH fluxes are taken into account, so the strengthened wet scavenging in summer may contribute to the decreases of the surface concentrations of PM_{10} as well. The surface reductions of PM_{10} induced by adding AH in the PRD region are smaller than those reported by Xie et al. (2016) in the Yangtze River Delta (YRD) region, which may attributed to the facts that the particle pollution is more severe and the AH emissions as well as their effects on meteorology are more obvious in the YRD region.

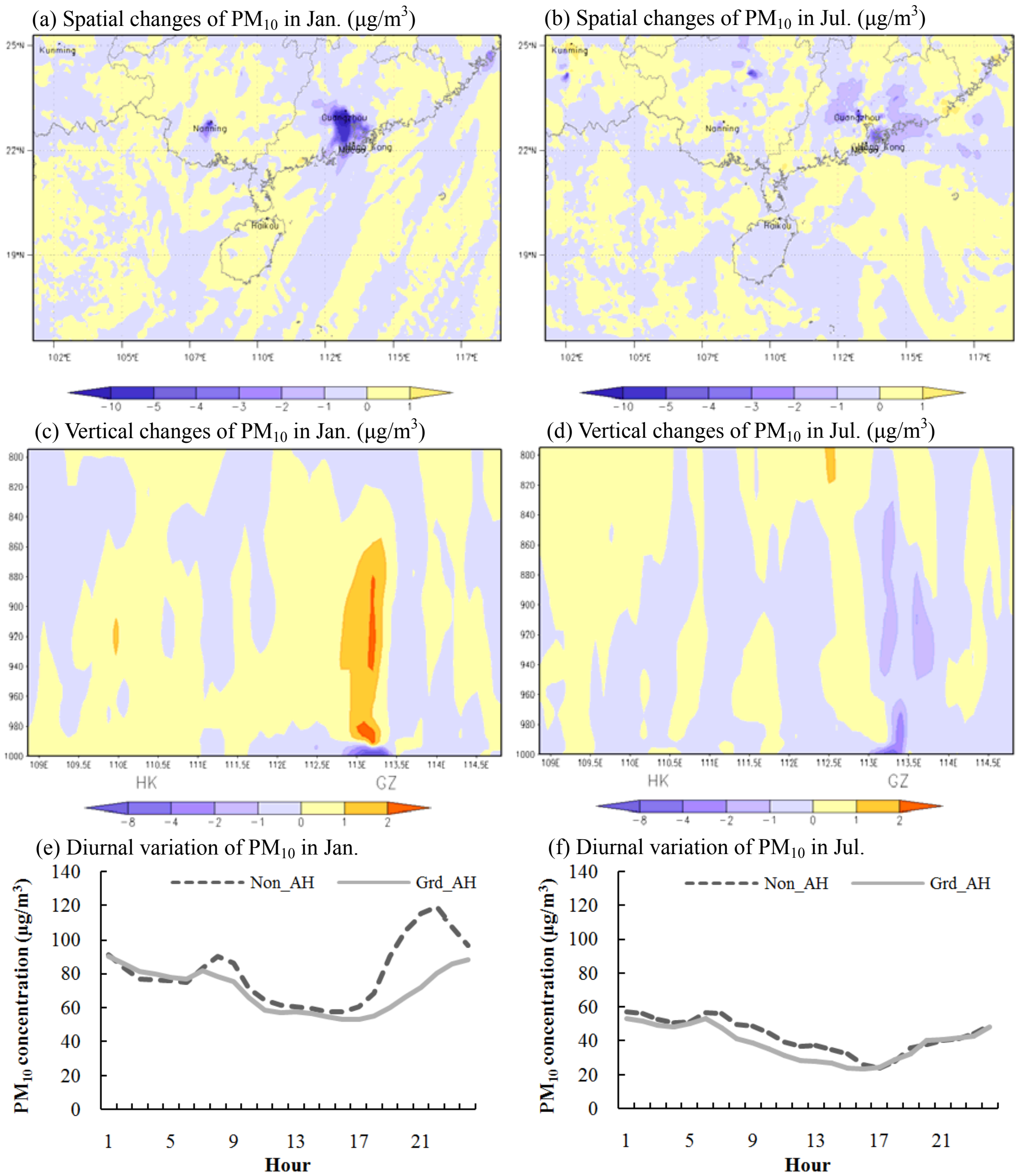

Fig. 8 Impacts of AH fluxes on the concentrations of PM_{10}: (a), (b) the spatial distribution of monthly-averaged differences for PM_{10} between Grd_AH and Non_AH (Grd_AH minus Non_AH) at the surface layer; (c), (d) the vertical distribution of monthly-averaged differences for PM_{10} between Grd_AH and Non_AH (Grd_AH minus Non_AH) from the surface to the 800hPa layer along the line AB shown in Fig. 1b; (e), (f) the monthly-averaged diurnal variations for PM_{10} concentrations over the urban areas in Guangzhou. Grd_AH and Non_AH represent the simulations with and without AH fluxes. (a), (c), and (e) show changes in January, while (b), (d), and (f) illustrate variations in July. In (c) and (d), HK and GZ are the abbreviations for Haikou and Guangzhou, respectively.

Fig. 8c and d present the vertical plots for the changes of PM_{10} impacted by adding AH (Grd_AH minus Non_AH) on the cross-sectional line AB shown in Fig. 1b. With respect to the megacity Guangzhou, the AH fluxes can decrease the concentrations of PM_{10} near surface and increase those at the upper layers. This vertical change pattern of PM_{10} is quite similar to that of water vapor (Fig. 6e and f), indicating that it is a reflection of the changes in vertical transport pattern due to AH (Yu et al., 2014; Xie et al., 2016). As shown in Fig. 8c for January, the decreases of PM_{10} manly confined at the surface, with the typical reductions over -8μg/m^3. Meanwhile, there are obvious increases of PM_{10} concentrations at the upper levels, with the increments over 2μg/m^3 from the 980hPa layer to the 850hPa layer (approximately from 500m to 1500m). But for July (Fig. 8d), from the surface to the 850hPa layer over Guangzhou, the PM_{10} concentrations are all reduced over -1μg/m^3, with the maximum values over -4μg/m^3 on the ground. The increasing zones only occur at the upper layers above 1.5km, with the increments over 1μg/m^3. This significant seasonal difference for the vertical distribution of PM_{10} changes over Guangzhou should be related with the fact that the atmosphere is more unstable and convective in summer than in winter, which can be further proven by the phenomenon that the enhanced upward air movement in July is stronger than that in January (shown in Fig. 6e and f). It should be noted that the vertical changes of PM_{10} in Haikou are indistinctive, implying that the surface air pollutants cannot be remarkably affected by adding AH if the heat emission fluxes are less than 10 w/m^2. Furthermore, the low particle pollution level may be another cause for the negligible vertical changes of PM_{10} in Haikou.

Fig. 8e and f show the monthly-averaged diurnal variations of surface PM_{10} from the Grd_AH and Non_AH simulations over the urban areas in Guangzhou. Obviously, the adding of AH fluxes can lead to the decrease of surface PM_{10} concentrations, with the daily mean value of -10.4μg/m^3 for January and -4.3μg/m^3 for July. There are significant differences between the impacts of AH in the daytime and those at night. In July (Fig. 8f), the decreases mainly occur from 6:00 to 17:00. In January (Fig. 8e), the decreases are -8.8μg/m^3 from 8:00 to 18:00 and -11.9μg/m^3 from 19:00 to 7:00, with the maximum reduction of -36.9μg/m^3 at 21:00. This pattern has a reverse correlation with the changes of PBLH shown in Fig. 7c and d, which also manifests the important role of vertical air movement in the changes of PM_{10}.

3.4.2 Changes of the spatial and vertical distribution of O_3

Fig. 9a and b present the effects of AH on the spatial distribution of O_3 at the surface layer over South China. The results show that the increases of surface O_3 level can be seen in megacities for both January and July. In January (Fig. 9a), the maximum O_3 differences occur in the big cities of the PRD region, with the monthly mean increment over 2.5ppb. In July (Fig. 9b), the increasing areas become larger, but with the high values close to 1 ppb in and around the cities. This changing pattern is similar to the findings reported in Seoul (Ryu et al., 2013), Beijing (Yu et al., 2014) and the cities in the YRD region (Xie et al., 2016).

Fig. 9c and d show the effects of AH on the vertical distribution of O_3 from the surface to the 800hPa layer along the line AB (illustrated in Fig. 1b). For the urban areas of Haikou, the vertical changes of O_3 are all within ±0.2 ppb, which means that low AH emissions in this city (<10w/m^2) cannot remarkably affected the physical and chemical formation of O_3. However, over the urban areas of big city Guangzhou, the vertical distribution of O_3 concentrations can be noticeably changed. In January (Fig. 9c), O_3 increases at the surface while decreases at the upper levels. The increases of O_3 concentrations are limited within 300m above the surface (<995hPa) over the urban areas, with the high values over 2.5 ppb. The maximum decreases of O_3 concentrations occur from the 990hPa layer to the 860hPa layer (approximately from 400m to 1500m), and the typical reductions are about 0.3 ppb. This change pattern in winter for Guangzhou is similar to the findings reported in Shanghai and Hangzhou (Xie et al., 2016). But for July, the vertical change pattern of O_3 above Guangzhou is totally different. As illustrated in Fig. 9d, O_3 concentrations decrease at the lower layers while increase at the upper levels. The decreases occur from the surface to the 850hPa layer (about 1.5 km) with the reduction values of -1 to -1.5ppb, and the increases appear at the upper layers as well as the surrounding air columns around Guangzhou with the increment about 0.9-1.2 ppb.

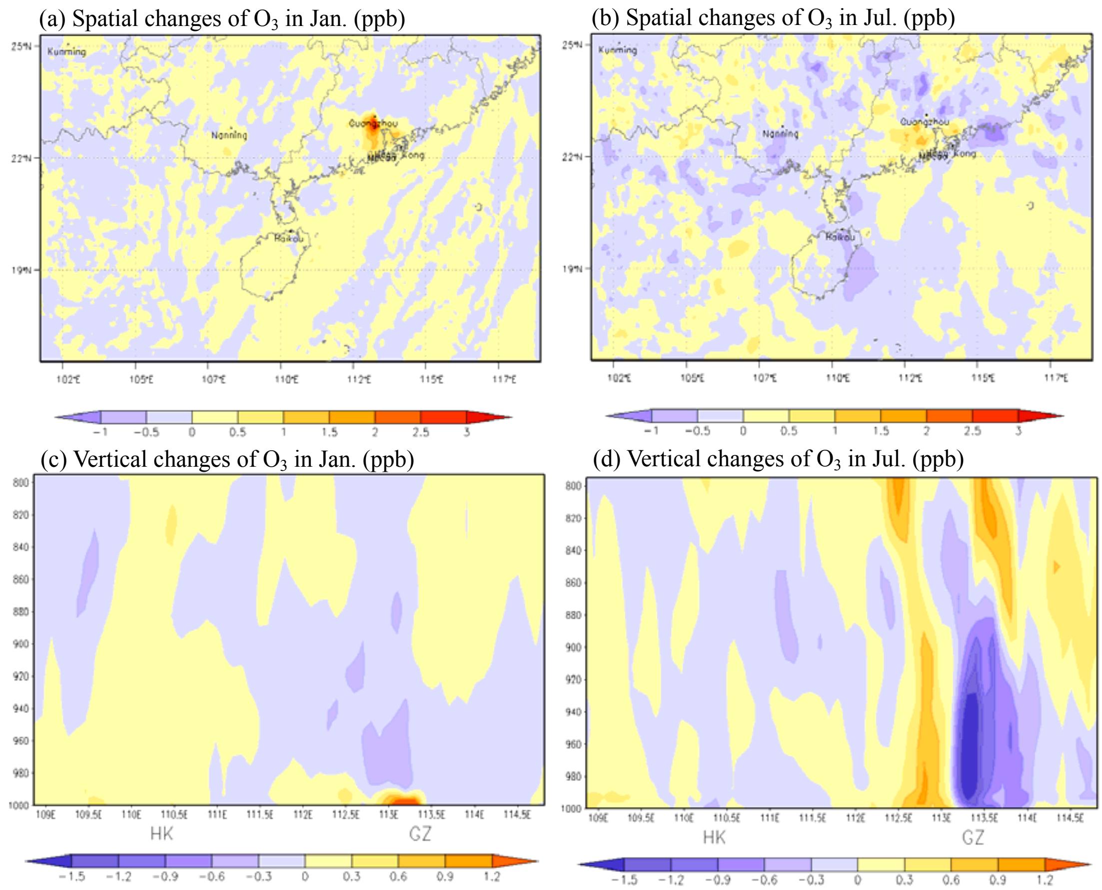

Fig. 9. Impacts of AH fluxes on the concentrations of O_3: (a), (b) the spatial distribution of monthly-averaged differences for O_3 between Grd_AH and Non_AH (Grd_AH minus Non_AH) at the surface layer; (c), (d) the vertical distribution of monthly-averaged differences for O_3 between Grd_AH and Non_AH (Grd_AH minus Non_AH) from the surface to the 800hPa layer along the line AB shown in Fig. 1b. Grd_AH and Non_AH represent the simulations with and without AH fluxes. (a) and (c) show changes in January, while (b) and (d) illustrate variations in July. In (c) and (d), HK and GZ are the abbreviations for

Haikou and Guangzhou, respectively.

The mechanism how the AH fluxes influence the spatial and vertical distribution of O_3 is more complicated than that for PM_{10}. Only taking the physical effects that just impact O_3 transport and dispersion into account, we can merely deduce that O_3 is seemingly reduced at the surface and may increase at the upper layers, because the increase of surface wind speed can facilitate O_3 advection transport and the rising up of PBLH can lead to O_3 dilution. However, O_3 is a secondary air pollutant produced by a series of complex chemical reactions that are also deeply affected by the ambient meteorological conditions. So, the chemical effects can play an important role in O_3 changes as well. For example, the increases of air temperature induced by adding AH can accelerate O_3 production rate. So it can directly increase the O_3 concentrations near the surface (referred to as the direct chemical effect hereafter). Moreover, because of the O_3 sensitivity in the daytime and the NO_x titration at night, O_3 formation is inextricably linked with NO_x (referred to as indirect chemical effect hereafter). As shown in Fig. 10, due mainly to the increases of PBLH and upward air flow caused by adding AH, NO_x can decrease at ground level and increase at upper layers in both January and July. Then when the process of NO_x titration predominate the O_3 chemistry at night, less NO_x consumes less O_3 and leaves more O_3 at the surface while more NO_x consumes more O_3 and reduce O_3 at the upper layers. For the daytime, because O_3 formation is sensitive to VOC over the cities in South China (Xie et al., 2014), the decrease in surface NO_x can lead to a slight increase in O_3 while the increase of NO_x at upper layers can result in the O_3 decrease. In January over Guangzhou, these direct and indirect chemical effects should play a more important role in O_3 changes than the physical effects, and thereby O_3 increases at ground level and decreases at upper layers. But in July, the physical effects should be the governing factor and cause the different pattern of O_3 changes in Guangzhou.

In the previous study on the O_3 variations induced by adding AH, it was found that the vertical changing patterns of O_3 over the YRD region in both January and July are always the same as the pattern shown in the winter of Guangzhou (Xie et al., 2016). Comparing the vertical changes of w for July in Guangzhou and those in Shanghai or Hangzhou, we can tell that the AH fluxes can induce stronger upward air movement in the cities of South China, which may be related with their special topographic and climatic features, and thereby more O_3 below the 850hPa layer is transported to the upper layers or to the surrounding areas of Guangzhou. On the other hand, the rise of air temperature is smaller in Guangzhou than those in the YRD cities, so there is no enough produced O_3 to compensate the loss of O_3 on the ground. Consequently, impacted by adding AH, O_3 decreases at the surface while increases at the upper layers in the summer of Guangzhou.

4. Conclusions

Anthropogenic heat (AH) fluxes related with the human activities can change the urban circulation and thereby affect the air pollution in and around cities. In this paper, we carry out systematic analyses to study the changes of meteorological conditions induced by AH and their effects on the concentrations of PM_{10}, NO_x and O_3 in South China. Firstly, the temporal and spatial distribution of AH emissions is estimated by a top-down energy inventory method. Secondly, the AH parameterization in WRF/Chem is modified to adopt the gridded AH data with the temporal variation. Finally, the WRF/Chem simulations are performed, and the differences between the cases with and without adding AH are analyzed to quantify the impacts of AH.

The results show that high AH fluxes generally occur in and around the cities. In 2014, the regional mean values of AH over Guangdong, Guangxi and Hainan province are 1.68, 0.44 and 0.49 W/m^2, while the typical values in the urban areas of the PRD region can reach 58.03w/m^2. The model results of WRF/Chem fit the observations well. Adding the gridded AH emissions can better describe the heterogeneous impacts of AH on regional meteorology and air quality. When AH fluxes are taken into account, the urban heat island and urban-breeze circulations in the big cities are significantly changed. In the PRD city cluster, 2-m air temperature rises up by 1.1℃ in January and over 0.5℃ in July, the boundary layer height increases by 120m in January and 90m in July, and 10-m wind speed is enhanced over 0.35 m/s in January and 0.3 m/s in July. The enhanced vertical movement can transport more moisture to higher levels, and causes the accumulative precipitation to increase by 20-40% over the megacities in July. Influenced by the modifications of meteorological conditions, the spatial and vertical distribution of air pollutants is modified as well. The concentrations of PM_{10} and NO_x decrease near surface while increase at the upper levels over the big cities in the PRD region, which are mainly related with the higher PBLH, stronger upward air flow, and higher surface wind speed. Because the direct chemical effect (the rising up of air temperature directly accelerates surface O_3 formation) and the indirect chemical effect (the decrease in NO_x at the ground results in the increase of surface O_3) play a more important role than the physical effects in winter, the surface O_3 concentrations can increase in January with maximum changes over 2.5ppb in the megacities. However, in July, the vertical changes of O_3 concentrations induced by adding AH show a different pattern, with reductions at the lower layers and increments at the upper layers over Guangzhou. This phenomenon should be attributed to the fact that the physical effects (enhanced upward movement caused by AH) become the dominant factor in summer.

There is an important question asked many times by scientists about whether anthropogenic heat emissions contribute to global warming. Although the answers are probably negative, the systematic analyses of AH over South China in this paper can enhance the understanding of the magnitude of AH emission from megacities and its impact on regional meteorology and atmospheric chemistry. Compared with the effects from urban land use (Wang et al., 2007; 2009b; Feng et al., 2012; Chen et al., 2014b; Li et al., 2014; 2016; Liao et al., 2015; Zhu et al., 2015), the impacts of AH are relative small. Especially in some cities with less air pollution and AH emissions, such as Haikou, the effects of AH on air quality may be ignored. But our results also clearly show that the meteorology and air pollution predictions in and around big cities are highly sensitive to the anthropogenic heat inputs. Thus, for further understanding of urban atmospheric environment issues, more studies of the anthropogenic heat release in megacities should be better considered.

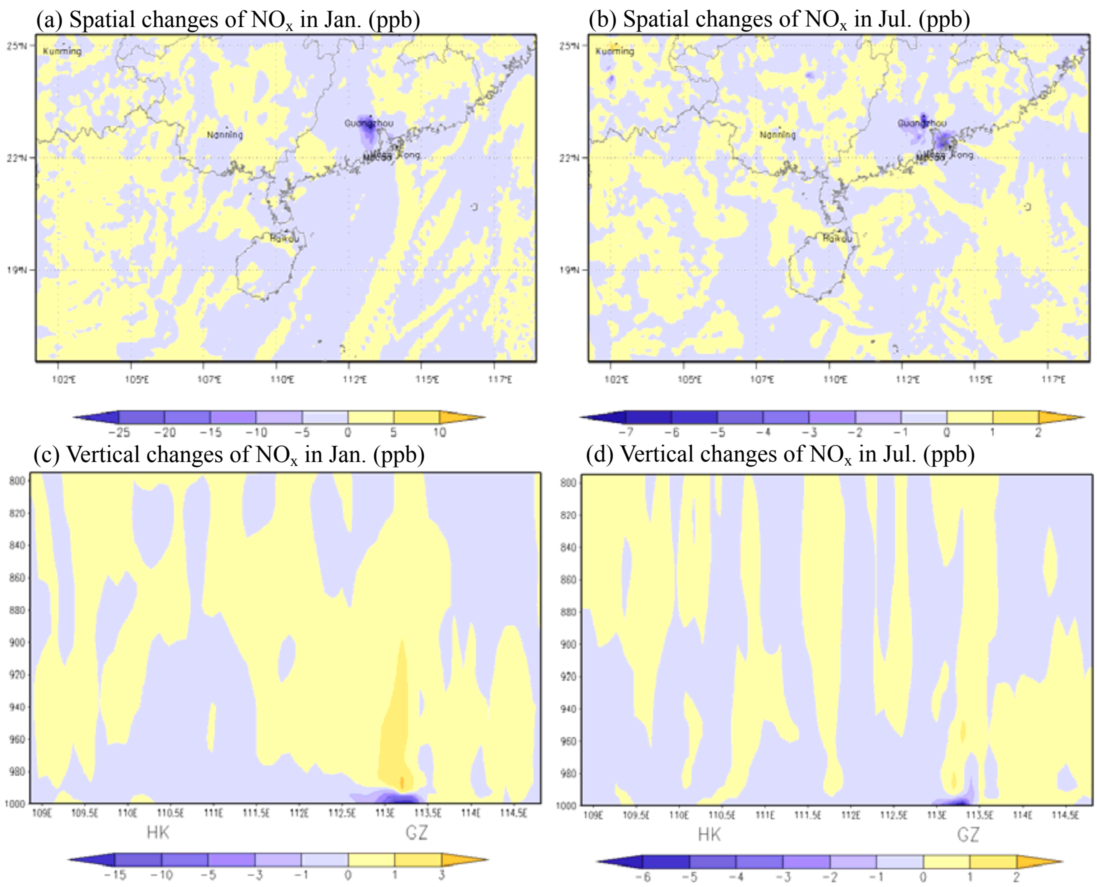

Fig. 10. Impacts of AH fluxes on the concentrations of NO_x: (a), (b) the spatial distribution of monthly-averaged differences for NO_x between Grd_AH and Non_AH (Grd_AH minus Non_AH) at the surface layer; (c), (d) the vertical distribution of monthly-averaged differences for NO_x between Grd_AH and Non_AH (Grd_AH minus Non_AH) from surface to 800 hPa layer along the line AB shown in Fig. 1b. Grd_AH and Non_AH represent the simulations with and without AH fluxes. (a) and (c) show changes in January, while (b) and (d) illustrate variations in July. In (c) and (d), HK and GZ are the abbreviations for Haikou and Guangzhou, respectively.

Acknowledgments

This work was supported by the National Natural Science Foundation of China (41475122, 91544230, 41621005), Key Laboratory of South China Sea Meteorological Disaster Prevention and Mitigation of Hainan Province (SCSF201401), the National Special Fund for Environmental Protection Research in the Public Interest (201409008), and EU 7th Framework Marie Curie Actions IRSES project REQUA (PIRSES-GA-2013-612671). The authors would like to thank the anonymous reviewers for their constructive and precious comments on this manuscript.

References

Ackermann, I. J., Hass, H., Memmesheimer, M., Ebel, A., Binkowski, F. S., and Shankar, U.: Modal aerosol dynamics model for Europe: Development and first applications, Atmos Environ, 32, 2981-2999, Doi 10.1016/S1352-2310(98)00006-5, 1998.

Akbari, H., Pomerantz, M., and Taha, H.: Cool surfaces and shade trees to reduce energy use and improve air quality in urban areas, Sol Energy, 70, 295-310, Doi 10.1016/S0038-092x(00)00089-X, 2001.

Allen, L., Lindberg, F., and Grimmond, C. S. B.: Global to city scale urban anthropogenic heat flux: model and variability, International Journal Of Climatology, 31, 1990-2005, 10.1002/joc.2210, 2011.

Balzarini, A., Pirovano, G., Honzak, L., Zabkar, R., Curci, G., Forkel, R., Hirtl, M., San Jose, R., Tuccella, P., and Grell, G. A.: WRF-Chem model sensitivity to chemical mechanisms choice in reconstructing aerosol optical properties, Atmos Environ, 115, 604-619, 10.1016/j.atmosenv.2014.12.033, 2015.

Block, A., Keuler, K., and Schaller, E.: Impacts of anthropogenic heat on regional climate patterns, Geophys Res Lett, 31, Artn L12211 10.1029/2004gl019852, 2004.

Bohnenstengel, S. I., Hamilton, I., Davies, M., and Belcher, S. E.: Impact of anthropogenic heat emissions on London's temperatures, Q J Roy Meteor Soc, 140, 687-698, 10.1002/qj.2144, 2014.

Chan, C. K., and Yao, X.: Air pollution in mega cities in China, Atmos Environ, 42, 1-42, 10.1016/j.atmosenv.2007.09.003, 2008.

Chen, F., and Dudhia, J.: Coupling an advanced land surface-hydrology model with the Penn State-NCAR MM5 modeling system. Part I: Model implementation and sensitivity, Mon Weather Rev, 129, 569-585, Doi 10.1175/1520-0493(2001)129<0569:Caalsh>2.0.Co;2, 2001.

Chen, Y., Jiang, W. M., Zhang, N., He, X. F., and Zhou, R. W.: Numerical simulation of the anthropogenic heat effect on urban boundary layer structure, Theor Appl Climatol, 97, 123-134, 10.1007/s00704-008-0054-0, 2009.

Chen, F., Kusaka, H., Bornstein, R., Ching, J., Grimmond, C. S. B., Grossman-Clarke, S., Loridan, T., Manning, K. W., Martilli, A., Miao, S. G., Sailor, D., Salamanca, F. P., Taha, H., Tewari, M., Wang, X. M., Wyszogrodzki, A. A., and Zhang, C. L.: The integrated WRF/urban modelling system: development, evaluation, and applications to urban environmental problems, International Journal Of Climatology, 31, 273-288, 10.1002/joc.2158, 2011.

Chen, B., Shi, G. Y., Wang, B., Zhao, J. Q., and Tan, S. C.: Estimation of the anthropogenic heat release distribution in China from 1992 to 2009, Acta Meteorol Sin, 26, 507-515, 10.1007/s13351-012-0409-y, 2012.

Chen, B., Dong, L., Shi, G. Y., Li, L. J., and Chen, L. F.: Anthropogenic Heat Release: Estimation of Global Distribution and Possible Climate Effect, J Meteorol Soc Jpn, 92A, 157-165, 10.2151/jmsj.2014-A10, 2014a.

Chen, B., Yang, S., Xu, X. D., and Zhang, W.: The impacts of urbanization on air quality over the Pearl River Delta in winter: roles of urban land use and emission distribution, Theor Appl Climatol, 117, 29-39, 10.1007/s00704-013-0982-1, 2014b.

Civerolo, K., Hogrefe, C., Lynn, B., Rosenthal, J., Ku, J. Y., Solecki, W., Cox, J., Small, C., Rosenzweig, C., Goldberg, R., Knowlton, K., and Kinney, P.: Estimating the effects of increased urbanization on surface meteorology and ozone concentrations in the New York City metropolitan region, Atmos Environ, 41, 1803-1818, 10.1016/j.atmosenv.2006.10.076, 2007.

Crutzen, P. J.: New Directions: The growing urban heat and pollution "island" effect - impact on chemistry and climate, Atmos Environ, 38, 3539-3540, 10.1016/j.atmosenv.2004.03.032, 2004.

Fan, H. L., and Sailor, D. J.: Modeling the impacts of anthropogenic heating on the urban climate of Philadelphia: a comparison of implementations in two PBL schemes, Atmos Environ, 39, 73-84, 10.1016/j.atmosenv.2004.09.031, 2005.

Fang, M., Chan, C. K., and Yao, X. H.: Managing air quality in a rapidly developing nation: China, Atmos Environ, 43, 79-86, 10.1016/j.atmosenv.2008.09.064, 2009.

Feng, J. M., Wang, Y. L., Ma, Z. G., and Liu, Y. H.: Simulating the Regional Impacts of Urbanization and

Anthropogenic Heat Release on Climate across China, J Climate, 25, 7187-7203, 10.1175/Jcli-D-11-00333.1, 2012.

Feng, J. M., Wang, J., and Yan, Z. W.: Impact of Anthropogenic Heat Release on Regional Climate in Three Vast Urban Agglomerations in China, Adv Atmos Sci, 31, 363-373, 10.1007/s00376-013-3041-z, 2014.

Ferguson, G., and Woodbury, A. D.: Urban heat island in the subsurface, Geophys Res Lett, 34, Artn L23713 10.1029/2007gl032324, 2007.

Flanner, M. G.: Integrating anthropogenic heat flux with global climate models, Geophys Res Lett, 36, Artn L02801 10.1029/2008gl036465, 2009.

Grell, G. A., and Devenyi, D.: A generalized approach to parameterizing convection combining ensemble and data assimilation techniques, Geophys Res Lett, 29, Artn 1693 10.1029/2002gl015311, 2002.

Grell, G. A., Peckham, S. E., Schmitz, R., McKeen, S. A., Frost, G., Skamarock, W. C., and Eder, B.: Fully coupled "online" chemistry within the WRF model, Atmos Environ, 39, 6957-6975, 10.1016/j.atmosenv.2005.04.027, 2005.

Guenther, A., Karl, T., Harley, P., Wiedinmyer, C., Palmer, P. I., and Geron, C.: Estimates of global terrestrial isoprene emissions using MEGAN (Model of Emissions of Gases and Aerosols from Nature), Atmos Chem Phys, 6, 3181-3210, 2006.

Hamilton, I. G., Davies, M., Steadman, P., Stone, A., Ridley, I., and Evans, S.: The significance of the anthropogenic heat emissions of London's buildings: A comparison against captured shortwave solar radiation, Build Environ, 44, 807-817, 10.1016/j.buildenv.2008.05.024, 2009.

Iamarino, M., Beevers, S., and Grimmond, C. S. B.: High-resolution (space, time) anthropogenic heat emissions: London 1970-2025, International Journal Of Climatology, 32, 1754-1767, 10.1002/joc.2390, 2012.

Ichinose, T., Shimodozono, K., and Hanaki, K.: Impact of anthropogenic heat on urban climate in Tokyo, Atmos Environ, 33, 3897-3909, Doi 10.1016/S1352-2310(99)00132-6, 1999.

Janjic, Z. I.: The Step-Mountain Eta Coordinate Model - Further Developments Of the Convection, Viscous Sublayer, And Turbulence Closure Schemes, Mon Weather Rev, 122, 927-945, Doi 10.1175/1520-0493(1994)122<0927:Tsmecm>2.0.Co;2, 1994.

Jiang, X. Y., Wiedinmyer, C., Chen, F., Yang, Z. L., and Lo, J. C. F.: Predicted impacts of climate and land use change on surface ozone in the Houston, Texas, area, J Geophys Res-Atmos, 113, Artn D20312 10.1029/2008jd009820, 2008.

Kim, H. J., and Wang, B.: Sensitivity of the WRF Model Simulation of the East Asian Summer Monsoon in 1993 to Shortwave Radiation Schemes and Ozone Absorption, Asia-Pac J Atmos Sci, 47, 167-180, 10.1007/s13143-011-0006-y, 2011.

Lee, S. H., Song, C. K., Baik, J. J., and Park, S. U.: Estimation of anthropogenic heat emission in the Gyeong-In region of Korea, Theor Appl Climatol, 96, 291-303, 10.1007/s00704-008-0040-6, 2009.

Li, M. M., Song, Y., Huang, X., Li, J. F., Mao, Y., Zhu, T., Cai, X. H., and Liu, B.: Improving mesoscale modeling using satellite-derived land surface parameters in the Pearl River Delta region, China, J Geophys Res-Atmos, 119, 6325-6346, 10.1002/2014JD021871, 2014.

Li, M. M., Song, Y., Mao, Z. C., Liu, M. X., and Huang, X.: Impacts of thermal circulations induced by urbanization on ozone formation in the Pearl River Delta region, China, Atmos Environ, 127, 382-392, 10.1016/j.atmosenv.2015.10.075, 2016.

Liao, J. B., Wang, T. J., Jiang, Z. Q., Zhuang, B. L., Xie, M., Yin, C. Q., Wang, X. M., Zhu, J. L., Fu, Y., and Zhang, Y.: WRF/Chem modeling of the impacts of urban expansion on regional climate and air pollutants in Yangtze River Delta, China, Atmos Environ, 106, 204-214, 10.1016/j.atmosenv.2015.01.059, 2015.

Lin, Y. L., Farley, R. D., and Orville, H. D.: Bulk Parameterization Of the Snow Field In a Cloud Model, J Clim Appl Meteorol, 22, 1065-1092, Doi 10.1175/1520-0450(1983)022<1065:Bpotsf>2.0.Co;2, 1983.

Liu, M., Wang, H., Wang, H., Oda, T., Zhao, Y., Yang, X., Zang, R., Zang, B., Bi, J., and Chen, J.: Refined estimate of China's CO2 emissions in spatiotemporal distributions, Atmos Chem Phys, 13, 10873-10882, 10.5194/acp-13-10873-2013, 2013a.

Liu, Q., Lam, K. S., Jiang, F., Wang, T. J., Xie, M., Zhuang, B. L., and Jiang, X. Y.: A numerical study of the impact of climate and emission changes on surface ozone over South China in autumn time in 2000-2050, Atmos Environ, 76, 227-237, 10.1016/j.atmosenv.2013.01.030, 2013b.

Lo, J. C. F., Lau, A. K. H., Chen, F., Fung, J. C. H., and Leung, K. K. M.: Urban modification in a mesoscale model and the effects on the local circulation in the Pearl River Delta region, J Appl Meteorol Clim, 46, 457-476, 10.1175/Jam2477.1, 2007.

Lu, X., Chow, K. C., Yao, T., Lau, A. K. H., and Fung, J. C. H.: Effects of urbanization on the land sea breeze circulation over the Pearl River Delta region in winter, International Journal Of Climatology, 30, 1089-1104, 10.1002/joc.1947, 2010.

Lu, Y., Wang, Q. G., Zhang, Y. Y., Sun, P., and Qian, Y.: An estimate of anthropogenic heat emissions in China, International Journal Of Climatology, 36, 1134-1142, 10.1002/joc.4407, 2016.

Madronich, S.: Photodissociation In the Atmosphere .1. Actinic Flux And the Effects Of Ground Reflections And Clouds, J Geophys Res-Atmos, 92, 9740-9752, Doi 10.1029/Jd092id08p09740, 1987.

Menberg, K., Bayer, P., Zosseder, K., Rumohr, S., and Blum, P.: Subsurface urban heat islands in German cities, Sci Total Environ, 442, 123-133, 10.1016/j.scitotenv.2012.10.043, 2013.

Meng, W. G., Zhang, Y. X., Li, J. N., Lin, W. S., Dai, G. F., and Li, H. R.: Application Of Wrf/Ucm In the Simulation Of a Heat Wave Event And Urban Heat Island around Guangzhou, J Trop Meteorol, 17, 257-267, 10.3969/j.issn.1006-8775.2011.03.007, 2011.

Mirzaei, P. A., and Haghighat, F.: Approaches to study Urban Heat Island - Abilities and limitations, Build Environ, 45, 2192-2201, 10.1016/j.buildenv.2010.04.001, 2010.

Mlawer, E. J., Taubman, S. J., Brown, P. D., Iacono, M. J., and Clough, S. A.: Radiative transfer for inhomogeneous atmospheres: RRTM, a validated correlated-k model for the longwave, J Geophys Res-Atmos, 102, 16663-16682, Doi 10.1029/97jd00237, 1997.

Oke, T. R.: The Urban Energy-Balance, Prog Phys Geog, 12, 471-508, Doi 10.1177/030913338801200401, 1988.

Pigeon, G., Legain, D., Durand, P., and Masson, V.: Anthropogenic heat release in an old European agglomeration (Toulouse, France), International Journal Of Climatology, 27, 1969-1981, 10.1002/joc.1530, 2007.

Quah, A. K. L., and Roth, M.: Diurnal and weekly variation of anthropogenic heat emissions in a tropical city, Singapore, Atmos Environ, 46, 92-103, 10.1016/j.atmosenv.2011.10.015, 2012.

Rizwan, A. M., Dennis, Y. C. L., and Liu, C. H.: A review on the generation, determination and mitigation of Urban Heat Island, J Environ Sci-China, 20, 120-128, Doi 10.1016/S1001-0742(08)60019-4, 2008.

Ryu, Y. H., Baik, J. J., and Lee, S. H.: Effects of anthropogenic heat on ozone air quality in a megacity, Atmos Environ, 80, 20-30, 10.1016/j.atmosenv.2013.07.053, 2013.

Sailor, D. J., and Lu, L.: A top-down methodology for developing diurnal and seasonal anthropogenic heating profiles for urban areas, Atmos Environ, 38, 2737-2748, 10.1016/j.atmosenv.2004.01.034, 2004.

Schell, B., Ackermann, I. J., Hass, H., Binkowski, F. S., and Ebel, A.: Modeling the formation of secondary organic aerosol within a comprehensive air quality model system, J Geophys Res-Atmos, 106, 28275-28293, Doi 10.1029/2001jd000384, 2001.

Stockwell, W. R., Middleton, P., Chang, J. S., and Tang, X. Y.: The 2nd Generation Regional Acid Deposition Model Chemical Mechanism for Regional Air-Quality Modeling, J Geophys Res-Atmos, 95, 16343-16367, Doi 10.1029/Jd095id10p16343, 1990.

Stone, B.: Urban sprawl and air quality in large US cities, J Environ Manage, 86, 688-698, 10.1016/j.jenvman.2006.12.034, 2008.

Wang, X. M., Lin, W. S., Yang, L. M., Deng, R. R., and Lin, H.: A numerical study of influences of urban land-use change on ozone distribution over the Pearl River Delta region, China, Tellus B, 59, 633-641, 10.1111/j.1600-0889.2007.00271.x, 2007.

Wang, T., Wei, X. L., Ding, A. J., Poon, C. N., Lam, K. S., Li, Y. S., Chan, L. Y., and Anson, M.: Increasing surface ozone concentrations in the background atmosphere of Southern China, 1994-2007, Atmos Chem Phys, 9, 6217-6227, 2009a.

Wang, X. M., Chen, F., Wu, Z. Y., Zhang, M. G., Tewari, M., Guenther, A., and Wiedinmyer, C.: Impacts of Weather Conditions Modified by Urban Expansion on Surface Ozone: Comparison between the Pearl River Delta and Yangtze River Delta Regions, Adv Atmos Sci, 26, 962-972, 10.1007/s00376-009-8001-2, 2009b.

Wang, X. M., Liao, J. B., Zhang, J., Shen, C., Chen, W. H., Xia, B. C., and Wang, T. J.: A Numeric Study of Regional Climate Change Induced by Urban Expansion in the Pearl River Delta, China, J Appl Meteorol Clim, 53, 346-362, 2014.

World Bank Group: East Asia's changing urban landscape: measuring a decade of spatial growth, World Bank, Washington Dc, 2015.

Wu, J. B., Chow, K. C., Fung, J. C. H., Lau, A. K. H., and Yao, T.: Urban heat island effects of the Pearl River Delta city clusters-their interactions and seasonal variation, Theor Appl Climatol, 103, 489-499, 10.1007/s00704-010-0323-6, 2011.

Wu, K., and Yang, X. Q.: Urbanization and heterogeneous surface warming in eastern China, Chinese Sci Bull, 58, 1363-1373, 10.1007/s11434-012-5627-8, 2013.

Xie, M., Zhu, K. G., Wang, T. J., Yang, H. M., Zhuang, B. L., Li, S., Li, M. G., Zhu, X. S., and Ouyang, Y.: Application of photochemical indicators to evaluate ozone nonlinear chemistry and pollution control countermeasure in China, Atmos Environ, 99, 466-473, 10.1016/j.atmosenv.2014.10.013, 2014.

Xie, M., Zhu, K. G., Wang, T. J., Feng, W., Zhu, X. S., Chen, F., Ouyang, Y., Liu, Z. J.: Study on the distribution of anthropogenic heat flux over China, China Environmental Science, 35, 728-734, 2015.

Xie, M., Liao, J., Wang, T., Zhu, K., Zhuang, B., Han, Y., Li, M., Li, S. : Modeling of the anthropogenic heat flux and its effect on regional meteorology and air quality over theYangtze River Delta region, China, Atmos. Chem. Phys., 16, 6071-6089, 10.5194/acp-16-6071-2016, 2016.

Yu, M., Carmichael, G. R., Zhu, T., and Cheng, Y. F.: Sensitivity of predicted pollutant levels to anthropogenic heat emissions in Beijing, Atmos Environ, 89, 169-178, 10.1016/j.atmosenv.2014.01.034, 2014.

Zhang, D. L., Shou, Y. X., and Dickerson, R. R.: Upstream urbanization exacerbates urban heat island effects, Geophys Res Lett, 36, Artn L24401 10.1029/2009gl041082, 2009a.

Zhang, Q., Streets, D. G., Carmichael, G. R., He, K. B., Huo, H., Kannari, A., Klimont, Z., Park, I. S., Reddy, S., Fu, J. S., Chen, D., Duan, L., Lei, Y., Wang, L. T., and Yao, Z. L.: Asian emissions in 2006 for the NASA INTEX-B mission, Atmos Chem Phys, 9, 5131-5153, 2009b.

Zhang, Y. N., Xiang, Y. R., Chan, L. Y., Chan, C. Y., Sang, X. F., Wang, R., and Fu, H. X.: Procuring the regional urbanization and industrialization effect on ozone pollution in Pearl River Delta of Guangdong, China, Atmos Environ, 45, 4898-4906, 10.1016/j.atmosenv.2011.06.013, 2011.

Zheng, J. Y., Zhang, L. J., Che, W. W., Zheng, Z. Y., and Yin, S. S.: A highly resolved temporal and spatial air pollutant emission inventory for the Pearl River Delta region, China and its uncertainty assessment, Atmos Environ, 43, 5112-5122, 10.1016/j.atmosenv.2009.04.060, 2009.

Zhu, K., Blum, P., Ferguson, G., Balke, K. D., and Bayer, P.: The geothermal potential of urban heat islands, Environ Res Lett, 5, Artn 044002 10.1088/1748-9326/5/4/044002, 2010.

Zhu, B., Kang, H. Q., Zhu, T., Su, J. F., Hou, X. W., and Gao, J. H.: Impact of Shanghai urban land surface forcing on downstream city ozone chemistry, J Geophys Res-Atmos, 120, 4340-4351, 10.1002/2014JD022859, 2015.